IPST Technical Paper Series Number 537

Macroscopic Flow Structures in a Bubbling Paper Pulp-Water Slurry

K.E. Taylor, S.M. Ghiaasiaan, S.I. Abdel-Khalik, J.D. Lindsay, and J. George

September 1994

Submitted to
AIChE National Meeting
November 13–18, 1994
San Francisco, California

MACROSCOPIC FLOW STRUCTURES IN A BUBBLING PAPER PULP-WATER SLURRY

Kevin E. Taylor, S. Mostafa Ghiaasiaan, and S. I. Abdel-Khalik
George W. Woodruff School of Mechanical Engineering
Georgia Institute of Technology, Atlanta, GA 30332-0405
mostafa.ghiaasiaan@me.gatech.edu

Jeffrey D. Lindsay*, Johnathan George
Institute of Paper Science and Technology, Atlanta, GA 30318
*Presently at Kimberly-Clark Corp., 2100 Winchester Road, Neenah WI 54956
jlindsay@kcc.com

Submitted to AIChE National Meeting, Nov. 1994, San Francisco

ABSTRACT

Hydrodynamics of three-phase bubbling pools, composed of batch mixtures of water and paper fiber with air throughput, were experimentally studied. Air flow through quiescent liquids or slurries was studied with a vertical transparent test column. Three similar test series were performed using pure water, and water pulp mixtures with 1% and 2% consistency (fiber weight percent). Void fraction profiles were obtained using the gamma-ray densitometry technique. The observed flow patterns in the pulp suspensions were significantly different than pure water, and those reported in the literature for non-fibrous three-phase columns. Gas channeling was observed at all gas superficial velocities and pulp consistencies, leading to poor mixing and shorter gas residence times. Three-dimensional flocs resulting in

tortuous, three-dimensional bubble paths could be observed in the 2% consistency tests.

A vertical cocurrent flow system was also studied in which air and pulp suspensions or water could flow simultaneously. Gamma densitometry was applied to measure gas holdup profiles through the test section. Many of the aforementioned features were observed in the cocurrent flow column. Of particular importance is the increase in gas holdup that can occur as pulp superficial velocity is increased, due to a decrease in bubble aggregation. Bubbles that are hindered by the pulp network structure can be carried away by the bulk flow before other bubbles collide and aggregate with the impeded bubbles. As a result, there are fewer large bubbles that break through the network structure and escape with a small dwell time.

I. INTRODUCTION

Three phase flow systems in which a slurry is subjected to bubbling gas have applications in various chemical, petrochemical, and environmental recovery processes. Bubbling of a fibrous slurry, which is the subject of this paper, occurs in floatation deinking, a process crucial in paper recycling. Despite an extensive literature dealing with three-phase systems, the fundamental characteristics of such fiber-liquid-gas three-phase systems are poorly understood, and most of the development of floatation deinking for the pump and paper industry has relied on purely empirical methods.

In floatation deinking, an aqueous suspension of paper fibers contaminated with ink particles, typically 20 to 100 μm in size, is subjected to air bubbles. Although a variety of floatation systems have been designed and used, all these systems have common basic features. A floatation system begins with a mixing zone where a fast-moving fiber suspension is mixed with air. Interaction among the bubbles, the liquid, and the fiber results in the detachment of hydrophobic ink particles from the fiber and their attachment to the bubbles. To promote these interactions, effective mixing of bubbles and fiber, where the bubble size is minimized in order to maximize the effective interphase surface area, is crucial. Following removal of ink particles by the bubbles, the bubbles must be separated from the fiber. This can be achieved by promoting bubble coalescence, which leads to the formation of larger, more buoyant bubbles. The bubbles carry the ink to the slurry surface where steady removal is achieved by skimming or overflow.

On a fundamental, microscopic scale, the liquid-fiber-bubble-ink particle interactions can be very complicated, and has not been adequately studied in the past. Such interactions, nevertheless, are expected to be strongly influenced by the

flow field hydrodynamics. The hydrodynamic attributes crucial to the performance of floatation deinking systems include:

1. Gas volume fraction and its distribution
2. Bubble size characteristics
3. Macroscopic flow field characteristics (bubble rise path, recirculation, channeling, etc.)

All these parameters have been extensively studied in the past in relation to two-and three-phase bubble columns and fluidized beds. Despite some similarities, however, the hydrodynamic characteristics of bubble columns and fluidized beds have limited direct applicability to fibrous pulp suspensions, as will be explained below. In the forthcoming review, we address primarily the literature dealing with air-water vertical columns without a throughput of water, which is relevant to much of the present study. For the low superficial velocities of pulp suspensions in this study and in general flotation deinking, studies of fluidized beds or other typical throughflow systems are usually of little value. We also discuss a few relevant studies of multiphase effects in fiber suspensions.

Three major flow regimes have been identified in two-phase bubble columns (Shah et al., 1982; Shenderov and Dilman, 1989) There is disagreement about conditions leading to switching from one regime to another, however, and these conditions may vary with system parameters. The bubbly regime is usually assumed to occur when superficial gas velocity, j_G, is less than 5 cm/s, and is characterized by dispersed bubbles ascending in roughly rectilinear paths, without significant interaction among themselves. Bubbles increasingly interact with each other and coalesce for 5 cm/s $\leq j_G \leq$ 10 cm/s, eventually leading to the establishment of the churn-turbulent regime for $j_G >$ 10 cm/s if column diameter, D_c, exceeds roughly 15 cm. In the latter regime large irregular-shaped bubbles, occasionally made of globules of smaller bubbles, account for most of the gas transport in the

pool (Shah et al., 1982; Godbole et al., 1982; Shah et al., 1985; Shenderov and Dilman 1989). In columns with D_c< roughly 15 cm, furthermore, a slug flow may develop instead of the churn-turbulent regime, where Taylor bubbles with diameters nearly equal to the column diameter dominate the flow field (one study, Ellis and Jones, 1965, suggests the critical column diameter may be closer to 7.5 cm). The aforementioned flow regimes are based on macroscopic, time-averaged measurements. A recent investigation of the instantaneous macroscopic flow characteristics in a 10.2-cm inner diameter air-water bubble column, by Chen et al. (1994), has revealed the occurrence of a complicated vortical-spiral central bubble stream in the bubbly-turbulent transition region.

Gas hold-up (void fraction) is a crucial parameter in bubble columns since a high void fraction implies larger total interfacial area and/or longer bubble residence time in the pool, both of which lead to higher volumetric transfer rates. Since the column wall effect becomes weak in large diameter columns supporting a churn-turbulent regime, the gas void fraction data may be extrapolated to much larger geometries from data obtained with small scale experiments, as long as D_c>15 cm (Shah et al., 1982). Many empirical correlations have thus been proposed (Akita and Yoshida, 1973; Bach and Pilhofer, 1978; Kumar et al., 1976; Hikita et al., 1980). The drift flux model (DFM) can also be applied (Wallis, 1969; Govier and Aziz, 1972). Bubble dynamics in bubble columns operating in the churn-turbulent regime are often simplified by dividing the bubbles into two size groups, large and small (Vermeer and Krishna, 1981; Godbole et al., 1982; Shah et al., 1985, Shenderov and Dilman, 1989). Bubble rise velocities for these two bubble groups have been measured using the dynamic gas disengagement technique by several investigators (Sriram and Mann, 1977; Vermeer and Krishna, 1981; Godbole et al., 1982; Shah et al., 1985; Shenderov and Dilman, 1989).

Although different flow regimes with distinct characteristics have also been observed and reported for three-phase systems (Zheng et al., 1988), many published investigations did not directly address flow regimes at all (Godbole et al., 1983; Shah et al., 1985; Sada et al., 1986; Chen and Fan, 1990). There also appears to be considerable disagreement among investigators with respect to the definition and characterization of flow regimes in three-phase systems (Zheng et al., 1988). Nevertheless, a simple flow-regime map similar to the two-phase bubble columns, consisting of a homogeneous bubbly zone at small j_G a transition zone at intermediate j_G and a turbulent bubbly zone at high j_G appears to be adequate (Zheng et al., 1988).

A large number of correlations and models have been proposed for predicting gas and liquid volume fractions in three-phase columns (see the review by Murayama and Fan, 1985). The drift flux model, modified to account for the effect of solid particles, has also been applied (Darton and Harrison, 1975; Chen and Fan, 1990; Sada et al., 1986). The processes that strongly affect hold-up are bubble wake hydrodynamics (Massimilla, 1959; Ostergaard, 1965; Darton and Harrison, 1975; Murayama and Fan, 1985), and particle-bubble interactions (Godbole et al., 1983). The presence of particles can in particular affect bubble coalescence and break-up. Contradictory results, however, have been reported, and it appears that particles which are wettable (i.e., have large contact angles with the liquid) augment bubble break-up, while non-wettable particles may help coalescence (Godbole et al., 1983).

The literature, represented by the above brief review, has limited applicability to pulp suspensions, however. Several important characteristics distinguish pulp suspensions from other three-phase systems. Isolated pulp particles, being fibrous, create non-Newtonian fluid characteristics in liquid-fiber mixtures (Bird et al., 1960). Pulp fibers, furthermore, have a density close to the

density of water and, when dispersed as isolated particles, can respond to local velocity gradients and turbulent eddies relatively fast. Most importantly, pulp fibers have the tendency to flocculate and form a network structure. Flocculation can take place in a water-pulp mixtures at consistencies as low as 0.5%, and for consistencies above roughly 1%, continuous fibrous networks form (Bennington et al., 1989). Network extent and strength increases with increasing consistency, creating local areas of high fiber concentration. Flocs can trap bubbles, preventing their rise through the suspension. Bubble streams must bypass flocs or coalesce into bubbles with enough buoyant force to break through the network. In stagnant pulp, bubbles are likely to flow through channels with lower hydraulic resistance.

Flocculation, even at low consistencies, renders the hydrodynamic characteristics of fibrous pulp mixtures quite different than those observed in other three-phase flow systems. At low shear, the network structure imparts a high apparent viscosity. Flocs may break up under shear, resulting in various macroscopic length scales in the fluid that yield complex friction loss curves for pipes. Under high shear, interaction of the fibers with fluid turbulence can lead to drag reduction (Lee and Duffy, 1976).

Serious research relevant to the hydrodynamics of fibrous pulp slurries has been reported only recently, and published studies are few. Walmsley (1992) performed experiments in 2-D (cylindrical) and 3-D (rectangular) transparent columns using batch fiber suspensions in the 0 - 2% consistency range. With the addition of only 0.1% wt pulp, he noticed significant hydrodynamic changes. He could recognize bubbly and churn flow regimes. Fibers were noticed to induce bubble coalescence, causing the development of churn flow at lower values of jG in comparison with a two-phase water-air bubbling pool.

Bubble characteristics in newsprint pulp were studied by Ajersch et al. (1992), who found bubble diameters to be approximately normally-distributed. Pelton and

Piette (1992) measured the probability of bubble escape through quiescent pulp suspensions in the 0.3% to 1.5% consistency range. Adhesion of bubbles to fibers was not observed. Instead, bubble entrapment in floc networks was noticed, and bubble escape occurred when bubble buoyancy overcame the network resistance.

Evidently, much more research is needed in order to understand the hydrodynamic characteristics of bubbling pulp slurries, and to establish a sound basis for designing these systems.

2. EXPERIMENTS

Figure 1 is a schematic of the quiescent liquid test apparatus, the main components of which are a cylindrical transparent column (the test section), an air flow system, and a gamma-ray densitometer and its electronics. The test section was a transparent cylinder with 12.7 cm inner diameter, 66 cm height, and 0.64 cm well thickness. Air was injected at the base of the column using a perforated rubber plate with approximately 230 holes. The holes were drilled with a 2.4 mm bit, and were arranged in a square lattice with 0.7 cm pitch. The air flow rate was measured using a Hastings Model PR-4A Four Channel Flow Meter.

Figure 2 shows the cocurrent flow system, which consists of a 1.5 m long transparent column with an internal diameter of 12.7 cm. Air and flowing slurry are mixed in a 2.5-cm pipe prior to a conical diffuser. A holding tank is used to separate air from the slurry before the slurry is pumped back to the test column.

The gamma-ray densitometer, used on both pulp systems, includes a 45 mCi Am-241 source and an Ortec Model 276 detector. Principles of gamma densitometry can be found elsewhere (Honan and Lahey, 1978; Vince and Finckle, 1983). The gamma-ray densitometer was used for measuring chord-average void fractions at various locations in the test section. To make this possible, a bracket was designed

and built to support the gamma source and the detector, which allowed for axial and lateral movement of the densitometer, ensuring that the collimated gamma beam and the detector remained aligned.

The heights at which gamma-ray densitometry was performed are designated as Planes h_0, h_1, etc., as shown in Figure 1. In the quiescent liquid apparatus, adjacent planes were 5.1 cm apart, and Plane h_0 was 8.9 cm above the test section bottom. Gamma-ray densitometry was performed on 9 chords in each measurement planes. The configuration of these chords is depicted in Figure 3, where the chord lengths are also given. Adjacent chords were approximately 1.3 cm apart.

The pulp slurry used in all pulp tests was produced from commercial unprinted newsprint composed primarily of southern softwood. The slurry was prepared by soaking the pulp in distilled water for several hours, followed disintegration at roughly 10% consistency in a laboratory repulper.

Before each test in the quiescent fluid apparatus, the test section was filled with four liters of water-pulp mixture at the desired consistency. The gamma-ray densitometer was calibrated for each of the aforementioned 45 chord locations (nine chords, five horizontal planes) separately. This was done by measuring the gamma beam attenuation twice, once with the test section empty, the other with the test section full with the water-pulp slurry (Honan and Lahey, 1978). Calibration measurements, as well as all gamma-ray densitometry measurements to be discussed later, were each repeated three separate times and then averaged. Similar procedures were applied for the cocurrent flow system, though longer averaging times were used for most runs rather than triple replication of gamma count measurements.

Following the completion of gamma-ray densitometer calibration, the air flow was adjusted at desired levels. The system was allowed to run for several minutes to ensure steady-state, and the gamma-ray densitometry measurements were

performed at all chordal locations. These measurements were repeated with pure water, and with 1% and 2% consistency water-pulp mixtures (2% consistency data are not available for the cocurrent flow system due to the difficulty of removing the entrained air from the pulp prior to recirculation).

An interesting characteristic of paper pulp suspensions, which makes them distinct from other slurries, is the former's capability to trap and maintain relatively significant amounts of gas, well after the flow of the throughput gas has been terminated. To study this phenomenon, a number of tests in the quiescent liquid apparatus were also performed to determine the effect of air superficial velocity during the operation of the apparatus on the amount of air that remained in the suspension mixture after the air flow was stopped. In each of these tests the air was initially allowed to flow at the desired rate for at least 30 seconds before the air flow was abruptly stopped. In order to allow for completion of bubble movement, gamma-ray densitometer counts were not recorded for at least 30 seconds after the air flow was stopped. Gamma-ray densitometry was then performed at all nine chord lengths at elevation h_2 (see Figures 1 and 3). These chord-average void fractions were then used in calculating the cross-sectional average void fraction on plane h_2, according to

$$\varepsilon_{G,j} = \frac{\sum_{i=1}^{9} \varepsilon_{G,i,j}\, \ell_i}{\sum_{i=1}^{9} \ell_i} \qquad (1)$$

where ε_G is the volume fraction of the gas (void fraction), and subscripts j and i are indices representing horizontal planes and chords depicted in Figures 1 and 3, respectively. For the aforementioned calculations of the void fraction at Plane h_2, j=2 in Equation 1.

The uncertainty associated with the gas hold-up measurement by gamma-ray densitometry was calculated using the methodology of Honan and Lahey (1978).

Accordingly, the calculated maximum relative errors, $\Delta\varepsilon_G/\varepsilon_G$, were 20% for ε_G = 0.015, 2% for ε_G = 0.11, and less than 1% for $\varepsilon_G \geq 0.22$.

The pool-average void fraction in the quiescent liquid tests could be obtained in two ways: by using the swell level height; or by volume-averaging the measured chord-average void fraction data from gamma-ray densitometry. These are explained below.

According to the first method, the pool-average void fraction was calculated from:

$$\bar{\varepsilon}_{G,SL} = 1 - H_o / H \tag{2}$$

where H_o represents the collapsed water level height in the column, and H represents the swell level height during the tests. Measurement of H was relatively simple for the pure water and pulp solutions at low air flow rates. At high j_G, however, the exact pool surface height was difficult to specify due to the waves resulting from frequent departures of large bubbles. For pure water tests the pool level height fluctuations resulted in an estimated maximum absolute uncertainties of $\Delta\bar{\varepsilon}_{G,SL} \approx \pm 0.02$. In tests with 1% and 2% consistency, the amplitudes of swell level height oscillations were larger, resulting in estimated maximum absolute uncertainties of $\Delta\bar{\varepsilon}_{G,SL} \approx \pm 0.03$.

In the second method of calculating the pool average void fraction, the volume-average void fraction representing the portion of the column below Plane h_4 (see Figure 1) was obtained from:

$$\bar{\varepsilon}_{G,h_4} = \frac{\sum_{j=o}^{4} \sum_{i=1}^{9} \varepsilon_{G,i,j}\, \ell_i}{5 \sum_{i=1}^{9} \ell_i} \tag{3}$$

3. RESULTS AND DISCUSSION

3.1 Pure Water Tests, Quiescent Liquid Apparatus

These tests were performed in order to provide a set of reference data to facilitate the interpretation of the tests with finite pulp consistency. Representative measured chord-average gas volume fraction profiles are depicted in Figures 4a through 4f, with ascending gas superficial velocities. The observed flow phenomena, to be briefly described below, were generally consistent with those reported by other investigators (Shah et al., 1982; Shenderov and Dilman, 1989).

Based on visual observations, for $j_G \leq 3$ cm/s the flow regime in the column was distinctly bubbly, and the system was characterized by a homogeneous mixture of bubbles rising along rectilinear paths. As noted in Figures 4a and 4b, except along chords a and b, which are strongly affected by the column walls, the chord-average ε_G is relatively uniformly distributed in the column. The flow regime in the 3 cm $\leq j_G \leq 6$ cm/s range represented transition from bubbly to churn-turbulent flow. With $j_G \geq 6$ cm/s the flow regime was distinctly churn-turbulent, characterized by the arrival of very large bubbles at the swell level. The churn-turbulent data, represented by Figures 4e and 4f, show a monotonic increase in ε_G with increasing chord length, indicating a nonuniform lateral distribution, and indicating higher ε_G near the center of the column. This lateral nonuniformity was evidently due to the formation of large, fast-moving bubbles near the center, which are formed due to strong bubble coalescence.

Recirculatory flow in a column or tank is easily established in the buoyant flow system of flotation deinking. The upward drag of the rising bubbles moves fluid upward, which must be replaced by fluid elsewhere moving downward. The injected gas tends to rise toward the center of a column with liquid flow returning downward at the walls of the column. (If a much wider column had been used, a set

of buoyant cells would be expected, with multiple regions of upward and downward flow.)

The churn-turbulent flow clearly supported a circulatory flow field in the column, in which small bubbles were noted to be entrained in the recirculating liquid near the column wall, and moved downward.

The column-averaged gas volume fractions, $\bar{\varepsilon}_{G,SL}$ and $\bar{\varepsilon}_{G,h_4}$, are depicted in Figure 5, where they are also compared with predictions of several widely-used empirical correlations. These correlations are presented in the Appendix. As noted, for $j_G \leq 1$ cm/s, where the flow regime is low-void fraction bubbly, there is good agreement between our data and all the correlations except for Hughmark (1967). Poor agreement between the data and all the correlations can also be noted for 3 cm/s $\leq j_G \leq$ 6 cm/s, representing the region of bubbly to churn-turbulent transition. In the churn-turbulent regime the data reasonably agree with the correlation of Kumar et al. (1976). Significant disagreement among various correlations, in particular at high j_G, is also noted.

The following are possible reasons for the relatively poor agreement between our data and the correlations depicted in Figure 4:

1. Bubble columns operating with air and water are divided into two broad categories (Shah et al., 1982). In large (D ≥ roughly 15 cm) columns, the churn flow regime is obtained at high gas superficial velocities, where gas hold-up is only weekly affected by the column size. In small columns (D<15 cm), on the other hand, slug flow dominated by large Taylor bubbles may occur at high gas superficial velocities. The above correlations are mostly based on data obtained with large columns. However, Taylor bubbles were not observed in the 13-cm columns of this study. In contrast to the 15-cm criteria of Shah, a study of Ellis and Jones (1965) in gas-liquid bubble columns indicates that gas holdup is not a function of column diameter for columns

greater than 7.5 cm in diameter. Gas holdup is increased by wall effects for more narrow columns.

2. All of the above correlations are based on data including relatively high superficial velocities. An exception is the correlation due to Kumar et al. (1976), for which the data base covers $j_G \leq 14$ cm/s.
3. The experimental data show relatively wide scatter, and are sensitive to the method of gas injection. Our data, for example, fall within the experimental data compiled and depicted by Bach and Pilhofer (1978).

3.2 Pulp Slurry Tests, Quiescent Liquid Apparatus

1% Consistency Pulp Results. Figures 6a through 6f depict representative profiles of chord-average void fractions for tests with 1% consistency pulp. Because of the opacity of the pulp slurry, visual observation of flow patterns and bubble hydrodynamic phenomena were limited to the regions adjacent to the column wall, and near the mixture swell level.

Visual observations indicated that the flow regime for the tests depicted in Figures 6a and 6b was bubbly. Comparing these figures with their pure water counterparts, Figures 4a and 4b, respectively, it can be noticed that the gas holdup values are generally lower than in water. Furthermore, unlike pure water, the data with 1% consistency show a monotonically increasing ε_G with height.

The decreased gas holdup due to the presence of fibers can be explained by the increased rate of coalescence induced by the fibrous network. Small bubbles, which normally have long dwell times, are impeded by the fiber network. A bubble held in place by a flow or network structure is soon joined by other rising bubbles, until coalescence yields a bubble with enough buoyant force to break through the restriction. At this point, the bubble begins to rise rapidly and can have a much smaller dwell time than the original small bubbles would have had in pure water.

The result is a net decrease in gas holdup (though Walmsley, 1992, also noted that fibers will increase gas holdup if the consistency is so dilute that flocs do not form). If the pulp consistency is high enough or if the gas flow rate is high enough, the gas may rise in distinct channels, resulting in very low residence time and low average holdup.

The increase in gas holdup with column height in an apparently bubbly flow of 1% pulp was not expected. The visual cues for a bubbly flow regime were probably misleading, for the fibrous slurry undoubtedly promoted coalescence, as evidenced by the lower gas holdup, but coalescence proceeds, larger bubbles and shorter dwell times are expected, resulting in a decrease in gas holdup with vertical height. However, recirculatory flow may partially account for the observed positive vertical gradient in ε_G. At the top of the column, fine air bubbles were formed in a froth, apparently due to natural or residual industrial surfactants in the pulp (some bubble dispersion by churning may have been present as well). These small bubbles can be carried back down into the flow by the descending fluid along the column walls. Recirculation ceases as the bottom of the column is approached, and the gas content of the descending fluid may decrease with decreasing height as fine bubbles coalesce and rise. These mechanisms could then impart an overall vertical gradient in gas holdup, with higher gas holdup near the surface of the slurry pool. It is possible that opposite trends or more uniform vertical distributions may be encountered, depending on the relative importance of churning, recirculation, and coalescence in the system.

Comparison between Figures 6a through 6f with their counterpart pure water test data in Figures 4a through 4f indicates generally lower, and considerably more non-uniform, void fractions in the former. The flow in the tests with 1% consistency slurry was noticeably more chaotic (with intense, turbulent churning) than those with pure water. High levels of churning throughout the column may have made

the vertical distribution of gas holdup more uniform in Figures 6d through 6f ($j_G > 5$ cm/s). The corresponding cases for water, Figures 4d through 4f, show positive vertical gradients in ε_G (increasing gas holdup with height) that may be attributed to slower coalescence, which in turn provides strong churning and a source of shear-dispersed bubbles only near the surface (as opposed to intense churning throughout the column). Fine bubbles induced by churning and sloshing near the surface can be carried downward by recirculatory flow.

In the tests represented by Figure 6a, because of the absence of strong recirculation in the lower section of the column, the fiber tended to build up at the column base and near the column wall. The resulting pulp formations, which are represented by the sketch in Figure 7, were responsible for the small values of chord-averaged ε_G values for chords a and b in Figure 6a. Such formations were also observed in the test represented by Figure 6b. They were, however, smaller and less frequent. These formations were not observed in other depicted tests, evidently due to the recirculatory flow patterns in these runs.

An unusual feature of the tests with 1% consistency pulp slurry was the presence of a thick foam layer on the pool surface. The thickness of the foamy layer increased as the air flow rate increased. The total amount of fiber trapped in the foamy layer, however, is believed to be small due to the very large gas volume fraction in such foamy mixtures. This effect, therefore, only slightly decreases the average consistency of the pulp slurry during the tests. The pool-average void fraction data presented elsewhere in this paper do not include this foamy layer.

2% Consistency Pulp Results. Representative chord-average void fraction profiles for tests in 2% consistency pulp are depicted in Figures 8a through 8f. These void fraction profiles are significantly different than void fraction profiles representing pure water and 1% consistency tests, and indicate entirely different

hydrodynamics. Once again, due to the opacity of the slurry, effective visual observations were limited to the vicinity of the swell level and the transparent column walls. These observations, along with the recorded void fraction profiles, indicated that the flow field in the column was dominated by the formation of three-dimensional pulp networks which resulted in the channeling phenomenon. Channeling could be seen along the column walls, as trains of large coalesced bubbles built up and rose along relatively well-defined and repeated paths. Bubble coalescence, which evidently occurred even at very low values of j_G, can be attributed to the fiber flocculation and the consequent channeling which also reduced the effective gas flow area. This reduction in flow area leads to higher gas velocities in the channels, leading to stronger bubble coalescence and the formation of large bubbles. Also, at low j_G, due to the absence of strong recirculation, the fibers tended to settle, causing an increase in the fiber consistency near the bottom of the test section.

Three dimensional flock networks, resulting in tortuous channels, are evident from the void fraction profiles for $j_G \leq 2$ cm/s (see Figures 8a and 8b). As j_G is increased, in Figures 8c through 8f, abrupt axial variations of chord-average void fractions become fewer, perhaps indicating reduction in the tortuosity of the channels. Channeling remains dominant, nevertheless, and strong lateral nonuniformity in ε_G persists. The channels appeared to form preferentially approximately half way between the column wall and its center.

There was little of the foaming action on the surface of the 2% pulp pool as seen on the surface of the 1% pulp pool surface.

3.3 Pool-Average and Residual Void Fractions

Plots of $\bar{\varepsilon}_{G,SL}$ and $\bar{\varepsilon}_{G,h_4}$, versus the superficial air velocity are given in Figures 9 and 10, respectively. Many empirical correlations have been suggested for predicting the pool-averaged gas or liquid volume fractions in three-phase

columns. Most of the correlations, however, only apply to fluidized beds and therefore deal with large solid particles significantly denser than the liquid phase, and are based on data with finite liquid superficial velocities (Murayama and Fan, 1985). These correlations are thus inapplicable to our data.

According to Figures 9 and 10 the presence of fibers results in significant reduction in pool-average void fraction, mainly due to the channeling phenomenon which also reduces mixing. In the experimental range, $\varepsilon_s \leq 2\%$, the average void fraction also monotonically decreases with increasing consistency, for all j_G values. The $\bar{\varepsilon}_G$ profiles for 1% and 2% consistencies both indicate that, for $j_G \geq 5$ cm/s, further increases in j_G result only in a slight increase in $\bar{\varepsilon}_G$.

The cross-sectional average residual void fractions representing Plane h_2 in Figure 1, are depicted in Figure 11. These void fractions, as mentioned before, were measured after the air flow was shut off, and represent entrapment of small air bubbles in the fibrous networks. Evidently, the bubble entrapment monotonically increases with increasing consistency and increasing the initial gas superficial velocity.

There was also a noticeable change in the distribution of the pulp fibers after the air flow was turned off. For the 1% pulp, the fibers would clump into regions of greater consistency. These regions appeared sphere shaped and had an average diameter of approximately 1 cm. For the 2% pulp, channels of lower consistency were visible after the termination of all air flow rates. The channels became better defined and greater in number as the initial air flow rate increased.

3.4 Cocurrent Flow Results

Unlike flow in the static column, the gas holdup in a 1% consistency pulp in the cocurrent flow system was generally found to be higher than the gas holdup in pure water at various combinations of liquid and gas flow rates. The reasons for this behavior are discussed later in this section. As a rule, flow regimes in the cocurrent

flow column resembled those in the quiescent column, with bubbly flow in water at low gas velocities (j_G roughly < 3 cm/s) followed by flow with a churn-turbulent nature at higher gas velocities. In pulp, the flow had a churn-turbulent nature at lower velocities, though only the outer portion of the flow could be seen (true for the quiescent column as well). What appeared to be churn-turbulent flow in some cases may have simply been in a transition regime from ideal bubble to churn-turbulent flow, for the gas holdup curves (holdup versus gas velocity) for pulp and for water were linear over the limited range of gas flow rates used. However, in pulp flows at the higher gas flow rates, some large bubbles were visible, with diameters on the order of 2-5 cm, which created large, swirling eddies in the flow as they rose, indicative of churn-turbulent flow. Precise identification of flow regimes in the future will require examination of transient differential pressure measurements across the column to obtain information not available by visual inspection.

To show that gas holdup has increased, in most cases, by the addition of fibers, we will consider $\bar{\varepsilon}_G$ (gas holdup values averaged over cross sectional area and over column height) as a function of j_G, as plotted in Figures 12-14. Part of the increased gas content in the pulp flow may be due to entrainment of air in the pulp as it flows from the holding tank back to the pump. For example, extrapolation in Figure 12 of the pulp curve to an injected gas flux of zero gives a holdup of 2%, indicating that 2% air content was present in the pulp as it left the holding tank. If so, the difference between the pulp and water results in Figure 12 may be due primarily to extra air that was present in the pulp before passing through the air injector. However, at higher liquid flow rates (Figures 13 and 14), the higher holdup in the pulp relative to water cannot be explained by higher initial air loading alone (in fact, the extrapolated air content at zero injected gas flux is about 2% for both water and pulp suspensions at the two higher pulp flow rates). In Figures 13 and 14, the liquid superficial velocity is greater than the gas superficial velocity for all measurements

(higher air flow rates increased pressure drop and increased air accumulation in the pump, hindering pump operation). Under these conditions, the dispersed bubbles, slowed in their ascent by the fibers, can be carried away by the pulp flow before other bubbles rise and coalesce with them. It seems that fibers cause coalescence when small bubbles cannot break through the network rapidly enough to avoid being hit by subsequent bubbles, and that aggregation continues until a large bubble has enough buoyant force to escape. When the pulp itself is flowing upwards as well, bubbles can avoid collisions by being carried away before later bubbles arrive.

Figures 15 through 19 show several examples (see George, 1994, for complete data sets) of radial and vertical variations observed in the chord-averaged gamma densitometry measurements through the cocurrent column for both pulp (1% ONP) and water at several liquid and gas fluxes. Both water and pulp results are similar, probably due to the decreased fiber-induced coalescence in the cocurrent flow. Flows at lower liquid velocity are more likely to have an uneven gas distribution in the lower portion of the column, probably due to the Coanda effect, causing the incoming flow to preferentially follow the wall of the conical expansion in some cases, or to oscillate from one side to the other. The gas distribution tends to be reasonably symmetric about the centerline after 80 cm of upward travel. The radial distribution of the chord-averaged gas holdup appears parabolic, commonly having a centerline average holdup two or three times the values at the wall. Since the centerline chord-average includes portions near the wall as well as at the center of the column, one might infer that the actual holdup at the center of the column is more than two or three times as great as the holdup at the walls. Using the assumption of radial symmetry, the chord averages at various radial locations can be used to solve for the true local radial holdup distribution that would yield the measured chord averages. Unfortunately, the inverse method (a matrix inversion) is relatively unstable, meaning that small changes in the measured chord averages

yield large changes in the symmetric radial distribution. Heavy smoothing of the actual data is usually required to avoid negative values in the radial solution. Where reasonable results were obtained, the calculated center gas holdup generally was three to seven times as great as the values near the wall, but this approach is questionable since most of our measurement show some departure from true radial symmetry.

Figure 15 provides an example for discussion. A superficial gas velocity of 3.1 cm/s flows in water having a superficial velocity of 2.5 cm/s. The air rising through the conical inlet probably fluctuates from side to side, yielding an apparent twin-peaked distribution in the time-averaged measurements near the inlet. The gas distribution becomes more symmetrical as the flow rises through the column. At 130 cm above the inlet, the radial distribution of chordal averages is nearly parabolic and on center. Chord-averaged centerline gas content is about twice that at the walls.

4. APPLICATIONS TO FLOTATION DEINKING

Though the present study represents an effort to understand basic phenomena at a level remote from the full complexities of true flotation deinking systems, several basic insights have been obtained with the following implications for flotation deinking:

1. Comparison of air flow through pulp suspensions and pure water show that fibers and flocs can induce significant changes in the spatial distribution of air, in bubble size distribution, and in the nature of the flow regime (e.g., bubbly, churn, churn-turbulent, channel flow). Unfortunately, much of the design of modern flotation deinking systems has been based on visualization studies in pure water, with the potential of inapplicable results. Undoubtedly, much room exists for improved flotation hydrodynamics.

2. Operators and vendors of flotation deinking cells have long known that flotation efficiency drops as pulp consistency exceeds a critical point (usually between 1 and 2%). Vendors have also learned that efficiency will decrease when the air flow rate is increased above a certain level. The fundamental causes for these drops in efficiency have not been clearly stated or even understood in the past. We now stress the importance of flow regimes in the behavior of flotation deinking. When consistency or gas flow rate are elevated, flow regimes with low interfacial area may be established (e.g., large bubbles or channel flow). Ink-bubble attachment and removal may then be reduced.
3. A buoyant driven flow such as occurs in flotation deinking may have strong recirculation, with fluid from the surface returning toward the bottom of the cell. This recirculation may be undesirable, for it can entrain ink-laden foam back into the suspension and can also backmix the deinked pulp into the dirty pulp. Recirculation will be tied to the geometry in a flotation unit. We expect more confined geometries would inhibit recirculatory flows. Wall effects (viscous shear) impede recirculation, for high shear would be required to have upward flow at the center and downward flow at the walls. Instead, wall effects may promote a more uniform flow and could increase the gas holdup and the interfacial area, though a transition to Taylor bubbles (slug flow) may occur if walls are too restricting. We can at least urge that novel flow geometries be considered to enhance flotation efficiency.
4. Cocurrent flow offers the potential for increased interfacial area and higher gas holdup by reducing floc-induced coalescence. This may be an important feature in some existing designs and may be further exploited as a design principle in the future.
5. The mechanisms that lead to large bubbles, especially that of floc-induced coalescence, suggests that the initial bubble size distribution entering a flow

system does not persist. The actual bubble size distribution in a flotation deinking cell may be only slightly linked to the original bubble size distribution. There is a need to develop techniques for determining the dynamic bubble size distribution in pulp slurries (student work is currently in progress on this important topic).

5. CONCLUSIONS

In the quiescent liquid apparatus, macroscopic flow patterns in three-phase pulp slurries with 1% and 2% consistency were experimentally studied, and were found to be significantly different than flow patterns observed in pure water or non-fibrous three-phase columns. Fiber flocculation and networking dominated the flow field. Gas channeling occurred at all gas superficial velocities and pulp consistencies, leading to poor mixing and shorter gas residence times. With 2% pulp consistency, three-dimensional flocs resulting in tortuous, three-dimensional bubble paths could be observed.

Similar tests in a cocurrent flow system with water and 1% pulp confirmed a number of the results obtained in quiescent liquid flow, while highlighting a mechanism for enhanced gas holdup when the liquid superficial velocity exceeds the gas superficial velocity. In this case, the bulk liquid flow may carry away gas bubbles before flocs induce significant coalescence into larger bubbles that would rise rapidly through the network, reducing the volumetric gas content.

Our experimental studies show that the hydrodynamics, and therefore transport processes, in three-phase pulp slurries may not be modeled by using the models and correlations based on non-fibrous data. Systematic experimental studies addressing three-phase fibrous systems are thus needed.

ACKNOWLEDGMENT

Thanks to Tom Merchant for assistance in experimental work, to Shawn Ye for assisting in construction of necessary apparatus, and to Michael Schaepe for expert assistance in the use of radioactive materials. Thanks to Mike Walmsley, Robert Pelton, and Chi Yu for useful suggestions and discussions. Portions of this work were conducted by Jonathan George in partial fulfillment of the requirements for the M.S. degree at IPST and by Kevin Taylor in partial fulfillment of the requirements for the M.S. degree at Georgia Tech. This work was funded by a research award from the TAPPI Research Foundation and by the member companies of IPST.

NOMENCLATURE

D_c = column diameter, m

g = gravitational acceleration, m/s^2

H_o = collapsed slurry level height (zero void fraction), m

H = bubbling slurry level height, m

I = index for chords in gamma-ray densitometry

j = superficial velocity, m/s; index for horizontal planes in the section

ℓ = chord length, m

Greek Letters

ε = gas volume fraction (void fraction)

$\Delta\bar{\varepsilon}_G$ = pool-average void fraction

$\Delta\bar{\varepsilon}_{G,h_4}$ = pool-average void fraction from Eq. 3

$\Delta\bar{\varepsilon}_{G,SL}$ = pool-average void fraction from Eq. 2

ε_s = pulp consistency (% wt of fiber in water-pulp mixture)

μ = dynamic viscosity, kg/m s

ρ = density, kg/m^3

σ = surface tension, N/m

Subscripts

G = gas phase

L = liquid phase

REFERENCES

Ajersch, M.; Pelton, R.; Towers, M.; Loewen, S. The Characterization of Dispersed Air in Two Newsprint Paper Machines. *J. Pulp Paper Sci.* **1992**, 18, 121.

Akita, K.; Yoshida, F. Gas Holdup and Volumetric Mass Transfer Coefficients in Bubble Columns. *Ind. Eng. Chem. Proc. Des. Dev.* **1973**, 12, 76.

Bach, H.F.; Pilhofer, T. Variations of Gas Hold-Up in Bubble Columns with Physics Properties of Liquids and Operating Parameters of Columns. *Ger. Chem. Eng.* **1978**, 1, 270.

Bennington, C.P.J.; Kerekes, R.J.; Grace, J.R. Mixing in Pulp Bleaching. *J. Pulp and Paper Sci.* **1989**, 15, 186.

Bird, R.B.; Stewart, W.E.; Lightfoot, E.N. *Transport Phenomena;* Wiley: New York, **1960**.

Chen, Y-M.; Fan, L-S. Drift Flux in Gas-Liquid-Solid Fluidized Systems from the Dynamics of Bed Collapse. *Chem. Eng. Sci.* **1990**, 45, 935.

Chen, R.C.; Reese, J.; Fan, L.-S. Flow Structure in Three-Dimensional and Three-Phase Fluidized Bed. *AIChe. J.*, **1994**, 7, 1093.

Darton, R.C.; Harrison, D. Gas and Liquid Hold-Up in the Three-Phase Fluidization. *Chem. Eng. Sci.* **1975**, 30, 581.

Duffy, G.G., and Titchener, A. L. Design Procedures for Obtaining Pipe Friction Loss for Chemical Pulps. *Tappi J.*, **1974**, 57, 162.

Ellis, J.E., and Jones, E.L. Two Phase Flow Symposium, Exeter, England, June 1965, as cited by Mashelkar, R. A. Bubble Columns. *British Chem. Eng.* **1970**, 15, 1297.

George, J. M.Sc. Thesis. Institute of Paper Science and Technology, Atlanta, Georgia, **1994**.

Godbole, S.P.; Honath, M.F.; Shah, Y.T. Holdup Structure in Highly Viscous Newtonian and Non-Newtonian Liquids in Bubble Columns. *Chem. Eng. Comm.* **1982,** 16, 119.

Godbole, S.P.; Schumpe, A.; Shah, Y.T. Hydrodynamics and Mass Transfer in Bubble Columns: Effect of Solids. *Chem. Eng. Comm.* **1983,** 24, 235.

Govier, G.W.; Aziz, K. *The Flow of Complex Mixtures in Pipes;* Robert E. Kreiger Publishing Co.: Malabar, Florida, **1972.**

Hikita, H.; Kikukawa, H. Liquid Phase Mixing in Bubble Columns. Effect of Liquid Properties. *Chem. Eng. J.* **1974,** 8, 191.

Hikita, H.; Asai, S.; Tanigawa, K.; Segawa, K.; Kita, M. Gas Hold-Up in Bubble Columns. *Chem. Eng. J.* **1980,** 20, 59.

Honan, T.J.; Lahey, R.T. The Measurement of Phase Separation in Wyes and Tees. U.S. Nuclear Regulatory Commission Rep. NUREG/CR-0557, **1978.**

Hughmark, G.A. Holdup and Mass Transfer in Bubble Columns, *Ind. Eng. Chem. Proc. Des. Dev.* **1967,** 6, 218.

Kumar, A.; Degaleesan, T.E.; Laddha, G.S.; Hoelsher, H.E. Bubble Swarm Characteristics in Bubble Columns. *Can. J. Chem. Eng.* **1976,** 54, 503.

Lee, P. F. W., and Duffy, G. G. Relationships Between Velocity Profiles and Drag Reduction in Turbulence Fiber Suspension Flow. *AIChE J.*, **1976,** 22, 750.

Murayama, K.; Fan, L.S. Fundamentals of Gas-Liquid-Solid Fluidization. *AIChE. J.*, **1985,** 13, 1.

Ostergaard, K. On Bed Porosity in Gas-Liquid Fluidization. *Chem. Eng. Sci.* **1965,** 20, 165.

Pelton, R.; Piette, R. Air Bubble Hold-Up in Quiescent Wood Pulp Suspensions. Can. *J. Chem. Eng.* **1992,** 70, 660.

Sada, E.; Kumazawa, H.; Lee, C.; Iguchi, T. Gas Holdup and Mass-Transfer Characteristics in a Three-Phase Bubble Column. *Ind. Eng. Chem. Proc. Des. Dev.* **1986**, 25, 472.

Shah, Y.T.; Kelkar, B.G.; Godbole, S.P. Design Parameters Estimation for Bubble Column Reactors. *AIChE J.* **1982**, 28, 353.

Shah, Y.T.; Joseph, S.; Smith, D.N.; Ruether, J.A. Two-Bubble Class Model for Churn-Turbulent Bubble-Column Reactor. *Ind. Eng. Chem. Proc. Des. Dev.*. **1985**, 24, 1096.

Shenderov, L.Z.; Dilman, V.E. Gas Motion in Bubble Reactors. *Theo. Found. Chem. Eng.* **1989**, 22, 359.

Sriram, K.; Mann, R. Dynamic Gas Disengagement: A New Technique for Assessing the Behavior of Bubble Columns. *Chem. Eng. Sci.* **1977**, 32, 571.

Taylor, K. An Experimental Investigation of a Bubbling Three-Phase Pool. MS Thesis, G. W. Woodruff School of Mechanical Engineering, Georgia Institute of Technology, **1993**.

Vermeer, D.J.; Krishna, R. Hydrodynamics and Mass Transfer in Bubble Columns Operating in the Churn-Turbulent Regime. *Ind. Eng. Chem. Des. Dev.* **1981**, 20, 475.

Vince, A.M., and Finckle, J. R. The Relationship Between Density and Void Fraction Measurement Uncertainty in Radiation Densitometry. *Int. J. Multiphase Flow*, **1983**, 9, 449.

Wallis, G. B. One-Dimensional Two-Phase Flow; McGraw Hill, New York, 1969.

Walmsley, M.R.W. Air Bubble Motion in Wood Pulp Fiber Suspension. *APPITA*. **1992**, 45, 509.

Zheng, C.; Yao, B.; Feng, Y. Flow Regime Identification and Gas Hold-Up of Three-Phase Fluidized Systems. *Chem. Eng. Sci.* **1988**, 43, 2195.

APPENDIX

Empirical correlations for pool-average gas volume fraction in two-phase bubble columns, and their important parameter ranges, are listed below.

Hughmark (1967)

j_G, m/s: 0.004 - 0.45, and D_C, m:>0.1

$$\bar{\varepsilon}_G = \frac{1}{2+(0.35/j_G)(\rho_L\sigma/0.072)^{1/3}} \tag{A-1}$$

(A04)

Hikita and Kikukawa (1974)

j_G, m/s: 0.042 - 0.38, D_C, m: 0.1 - 0.19, H, m: 0.6 - 1.35

$$\bar{\varepsilon}_G = 0.505 j_G^{0.47}(0.072/\sigma)^{2/3}(0.001/\mu_L)^{0.05} \tag{A-2}$$

Kumar et al. (1976)

j_G, m/s: 0.0014 - 0.14, D_C, m: 0.05 - 0.1

$$\bar{\varepsilon}_G = 0.728U - 0.485U^2 + 0.0975U^3 \tag{A-3}$$

$$U = j_G\left[\rho_L^2/\sigma(\rho_L - \rho_G)g\right]^{1/4} \tag{A-4}$$

Hikita et al. (1980)

j_G, m/s: 0.041 - 0.38, D_C, m: 0.1, H, m: 0.65

$$\bar{\varepsilon}_G = 0.672\left(\frac{j_G\mu_L}{\sigma}\right)^{0.578}\left(\frac{\mu_L^4 g}{\rho_L\sigma^3}\right)^{-0.131}\left(\frac{\rho_G}{\rho_L}\right)^{0.062}\left(\frac{\mu_G}{\mu_L}\right)^{0.107} \tag{A-5}$$

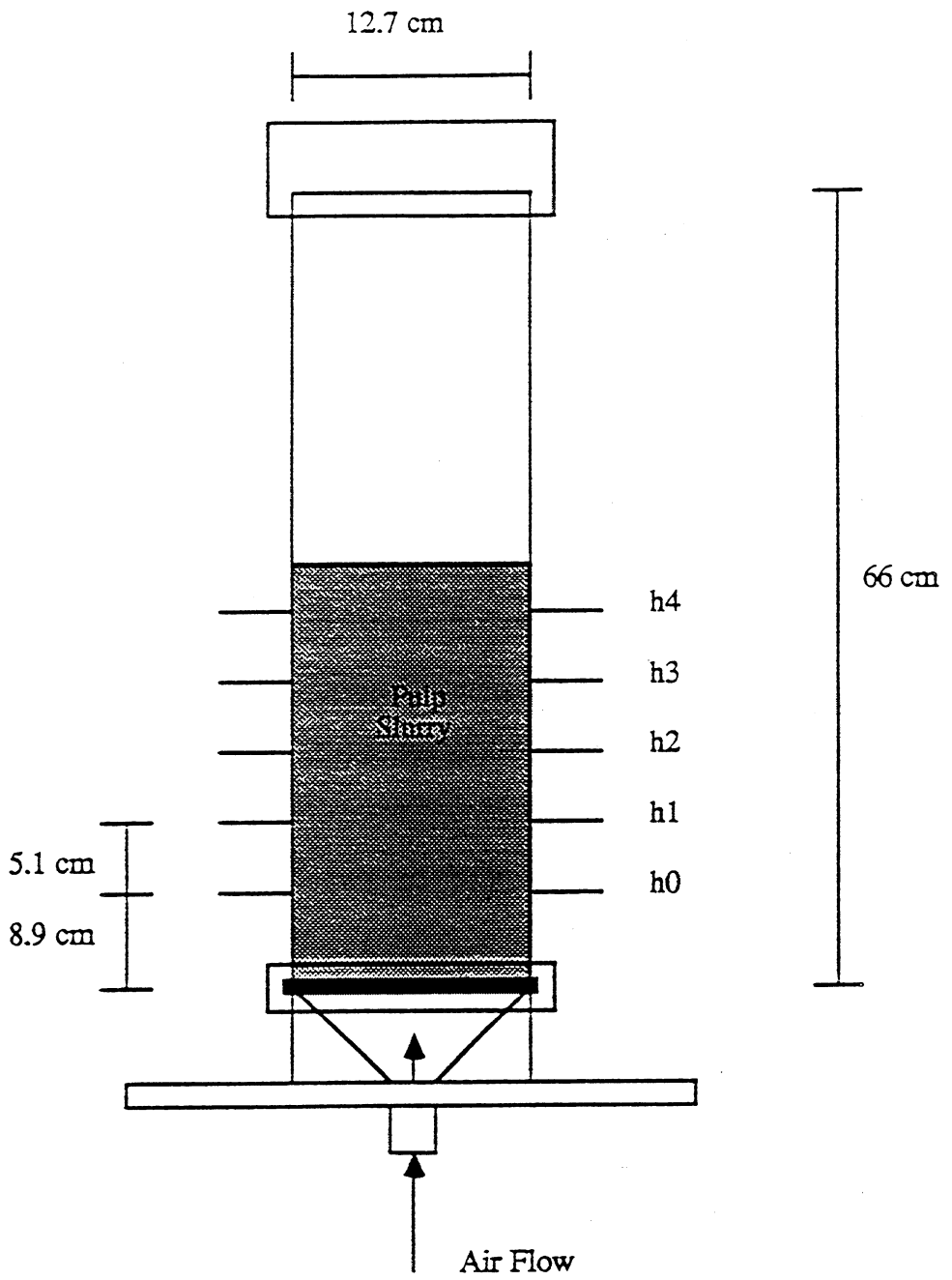

Figure 1. Quiescent liquid test facility.

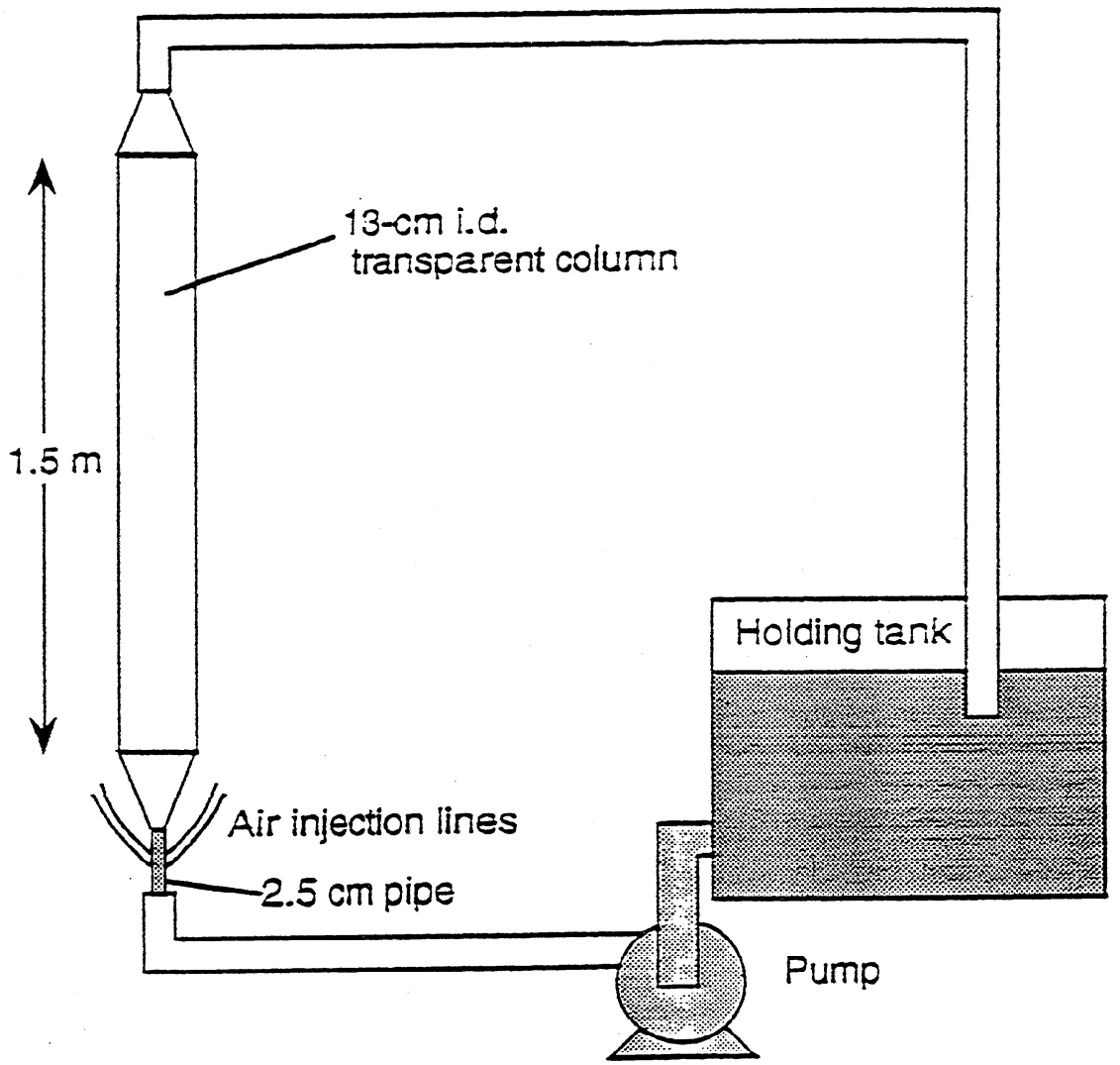

Figure 2. Cocurrent flow test facility.

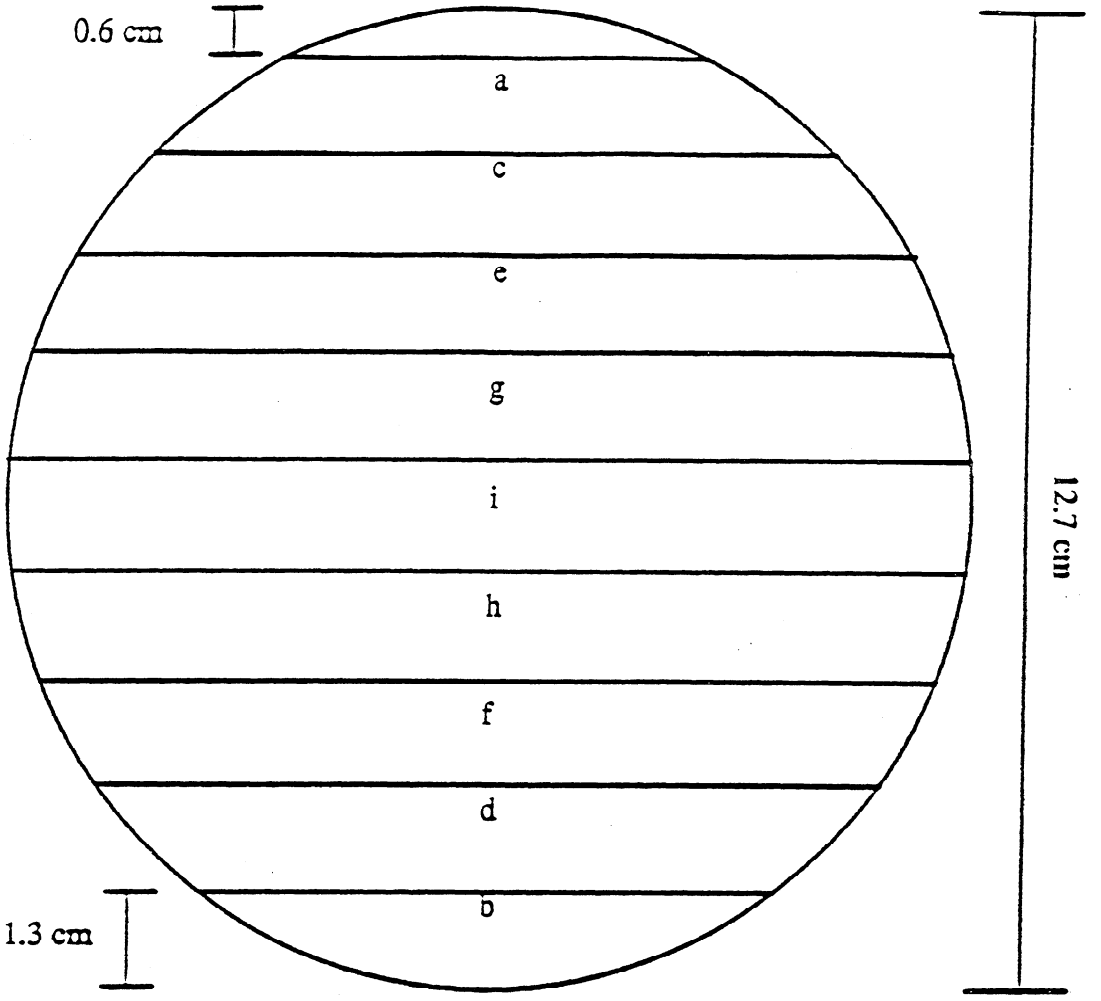

Channel Chord Lengths Examined

a = 5.1 cm
b = 7.8 cm
c = 9.0 cm
d = 10.3 cm
e = 10.9 cm
f = 11.9 cm
g = 12.0 cm
h = 12.5 cm
i = 12.7 cm

Figure 3. Chords selected for gamma-ray densitometry

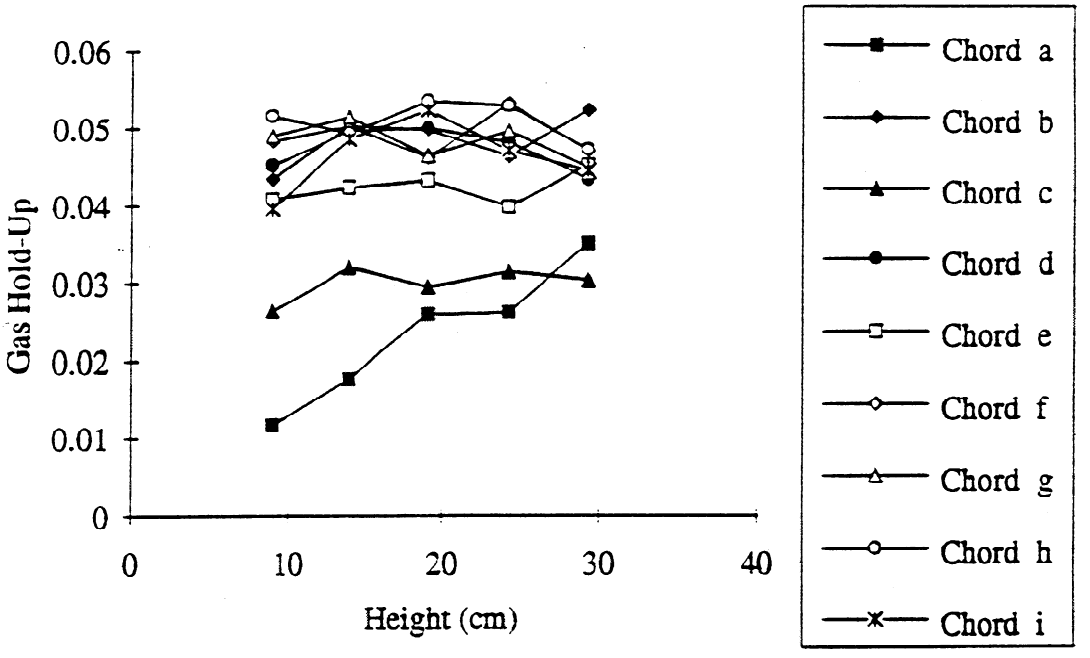

Gas holdup profiles in pure water, quiescent liquid apparatus.

Figure 4a. j_G = 0.79 cm/s

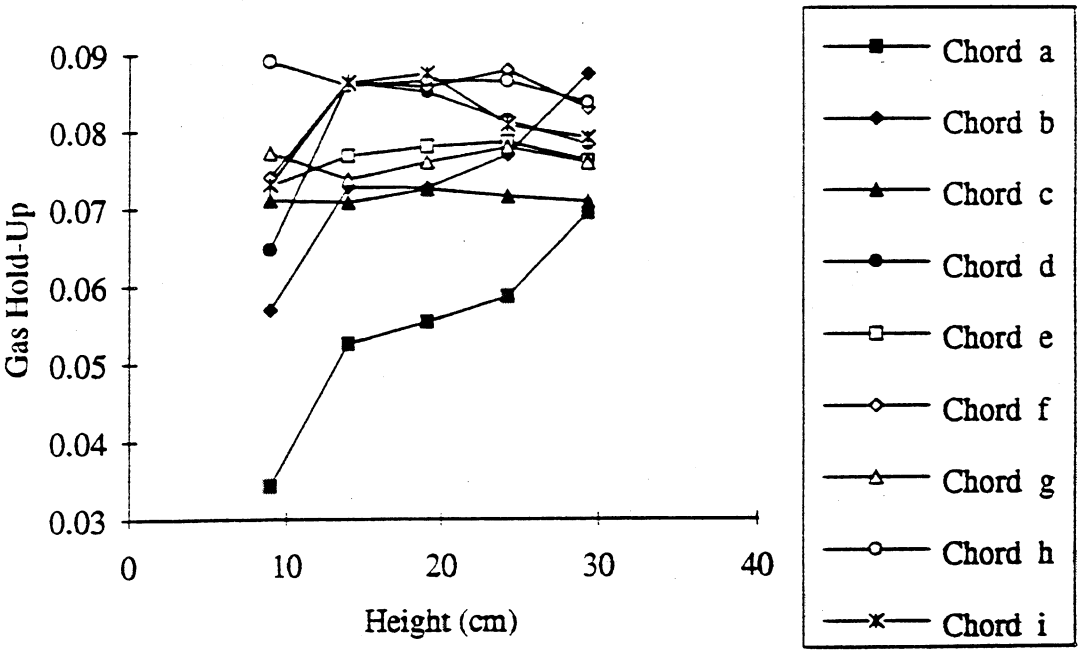

Gas holdup profiles in pure water, quiescent liquid apparatus.

Figure 4b. j_G = 1.32 cm/s

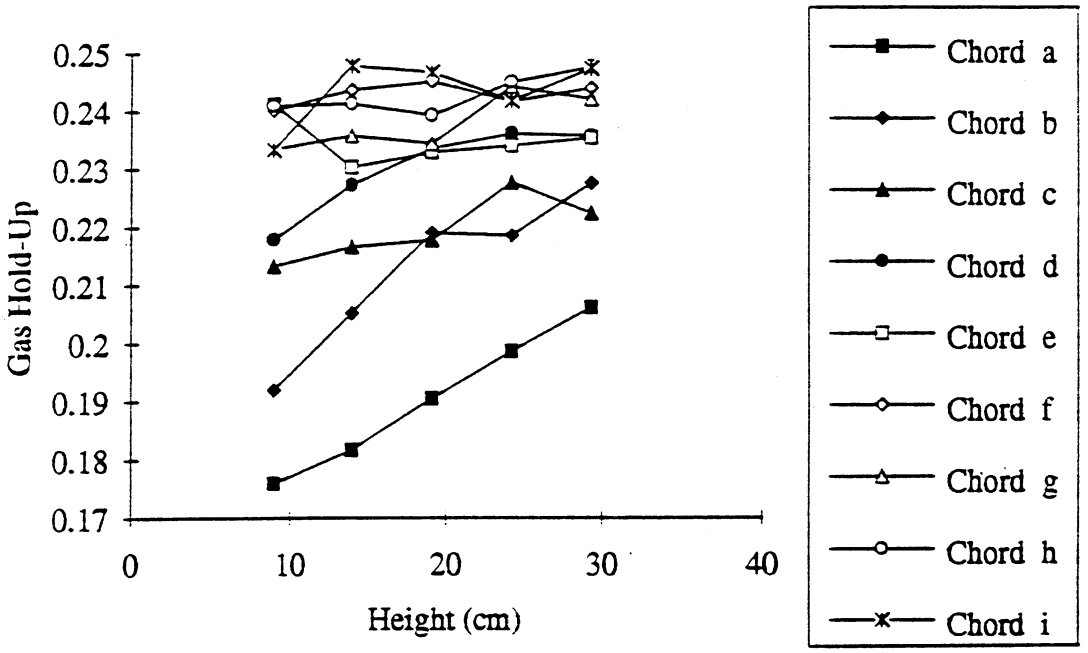

Gas holdup profiles in pure water, quiescent liquid apparatus.

Figure 4c. j_G = 3.95 cm/s

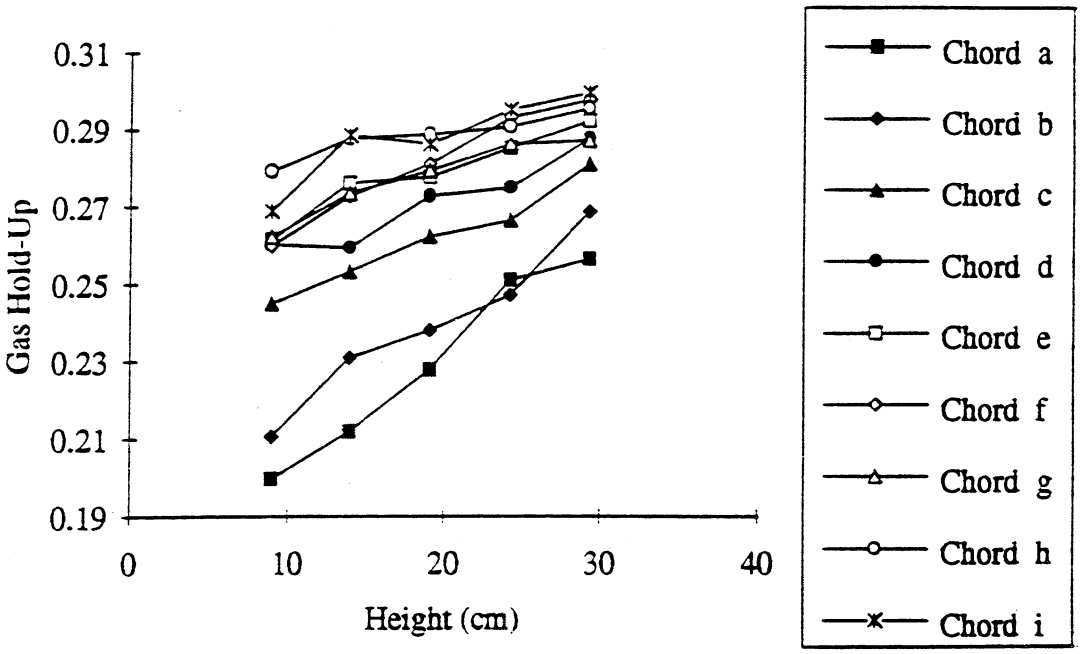

Gas holdup profiles in pure water, quiescent liquid apparatus.

Figure 4d. j_G = 5.26 cm/s

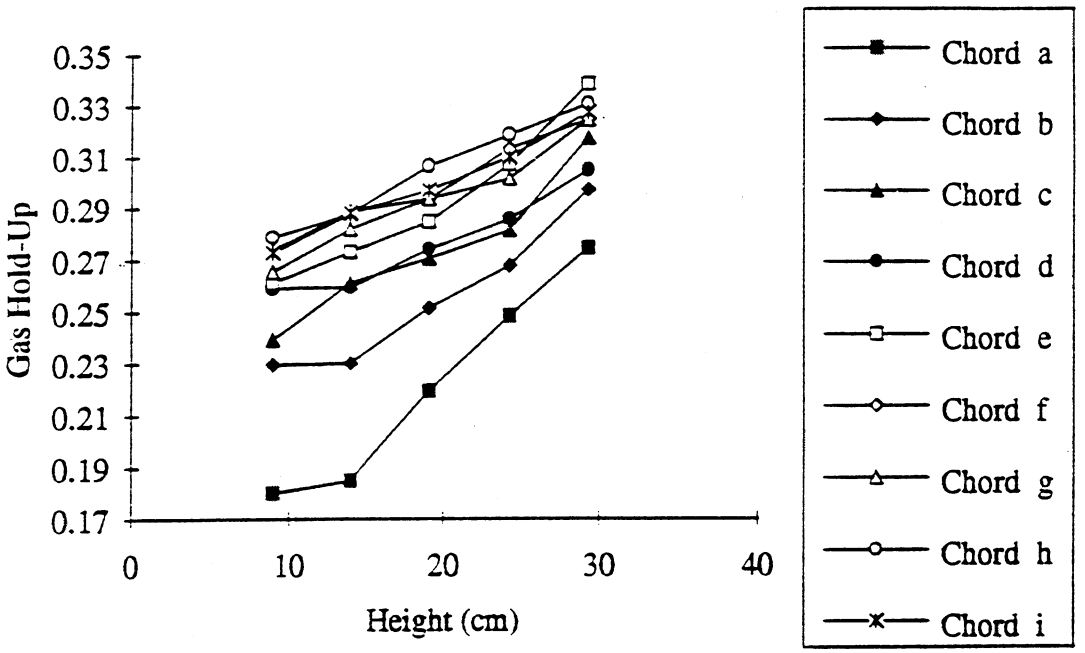

Gas holdup profiles in pure water, quiescent liquid apparatus.

Figure 4e. j_G = 6.58 cm/s

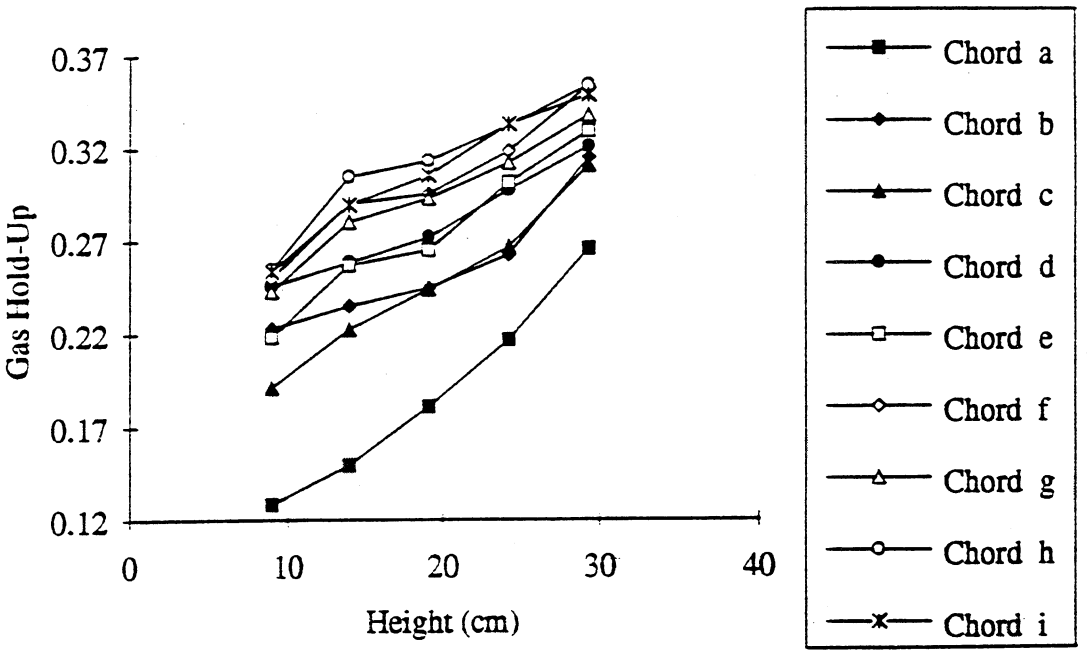

Gas holdup profiles in pure water, quiescent liquid apparatus.

Figure 4f. j_G = 9.21 cm/s

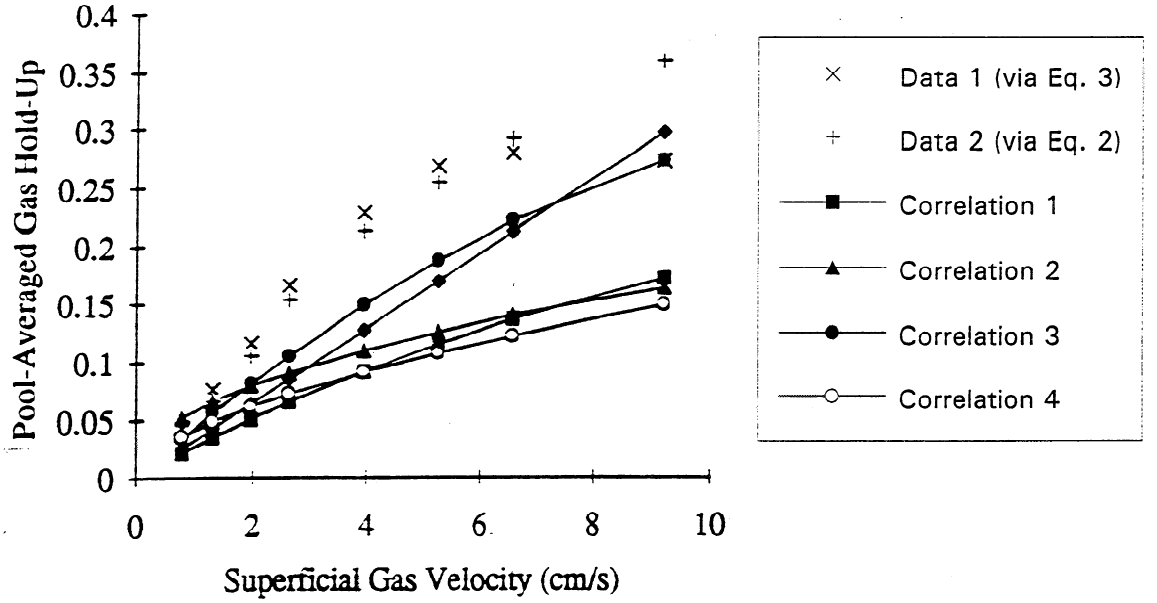

Figure 5. Pool-average gas holdup, air and water, quiescent liquid facility.

Correlations are given in the Appendix
Correlation 1: Hughmark (1967)
Correlation 2: Hikita and Kikukawa (1974)
Correlation 3: Kumar et al. (1976)
Correlation 4: Hikita et al. (1980)

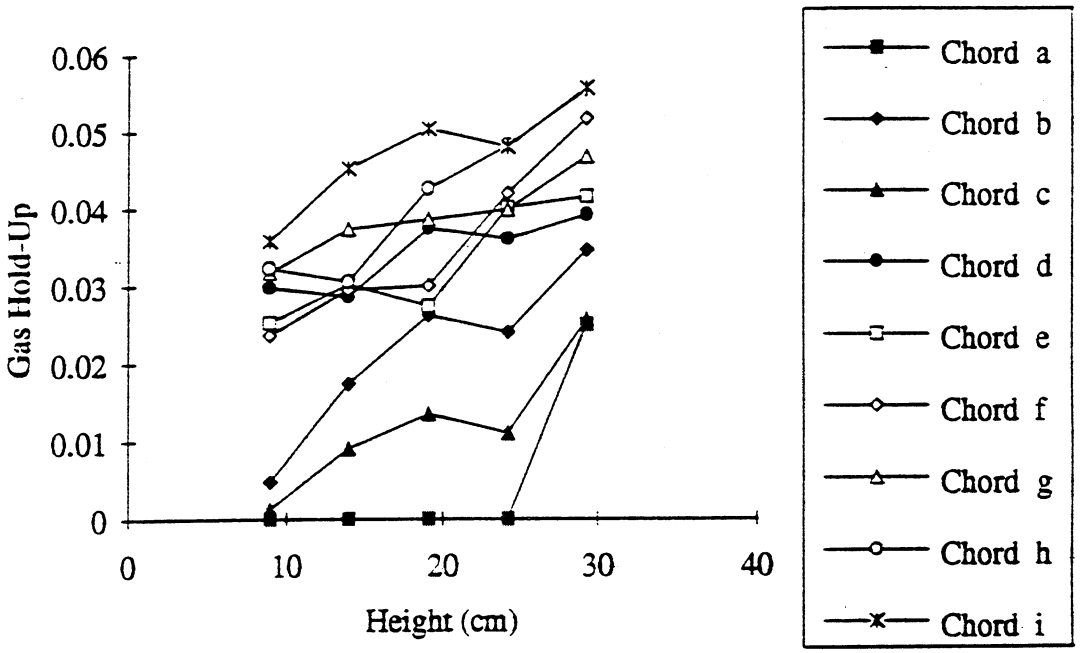

Gas holdup profiles in 1% consistency pulp, quiescent liquid apparatus.

Figure 6a. j_G = 0.79 cm/s

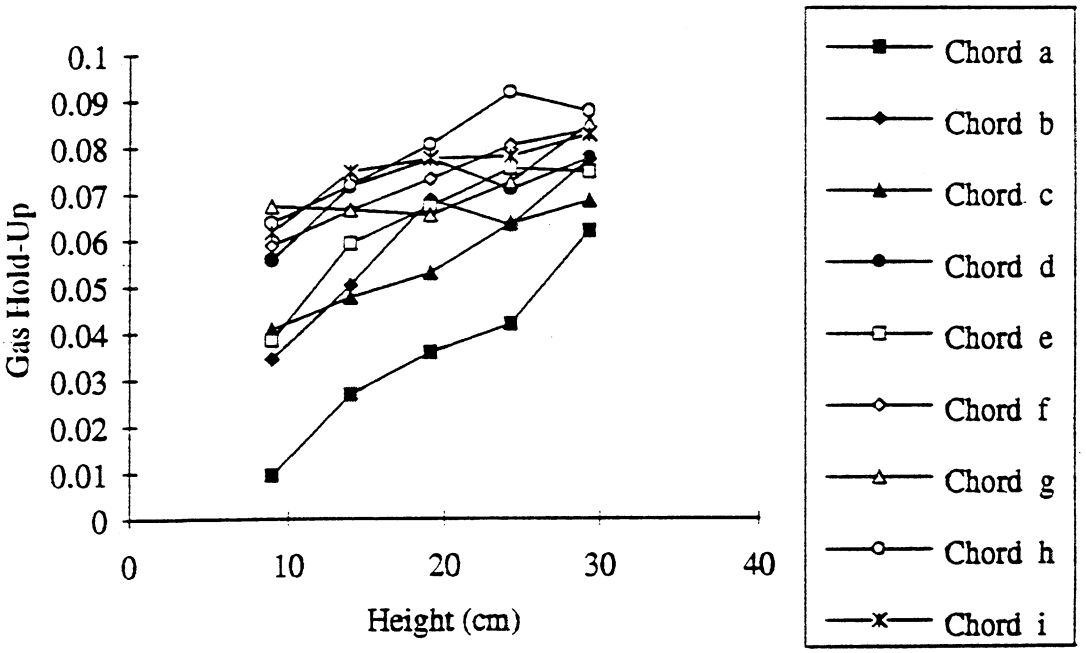

Gas holdup profiles in 1% consistency pulp, quiescent liquid apparatus.

Figure 6b. j_G = 1.32 cm/s

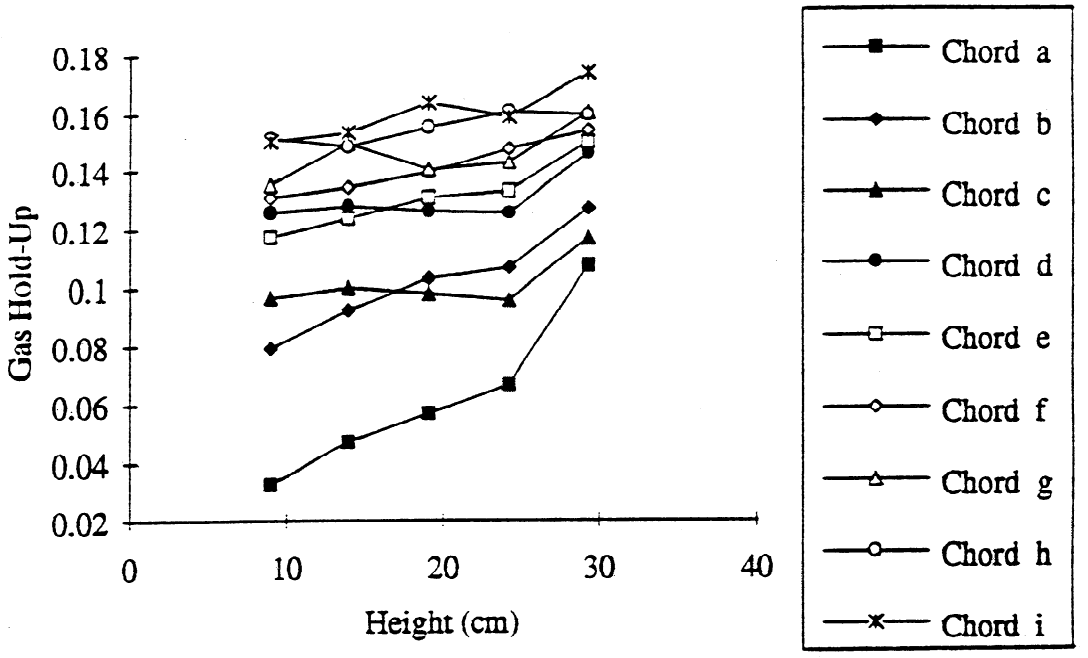

Gas holdup profiles in 1% consistency pulp, quiescent liquid apparatus.

Figure 6c. j_G = 3.95 cm/s

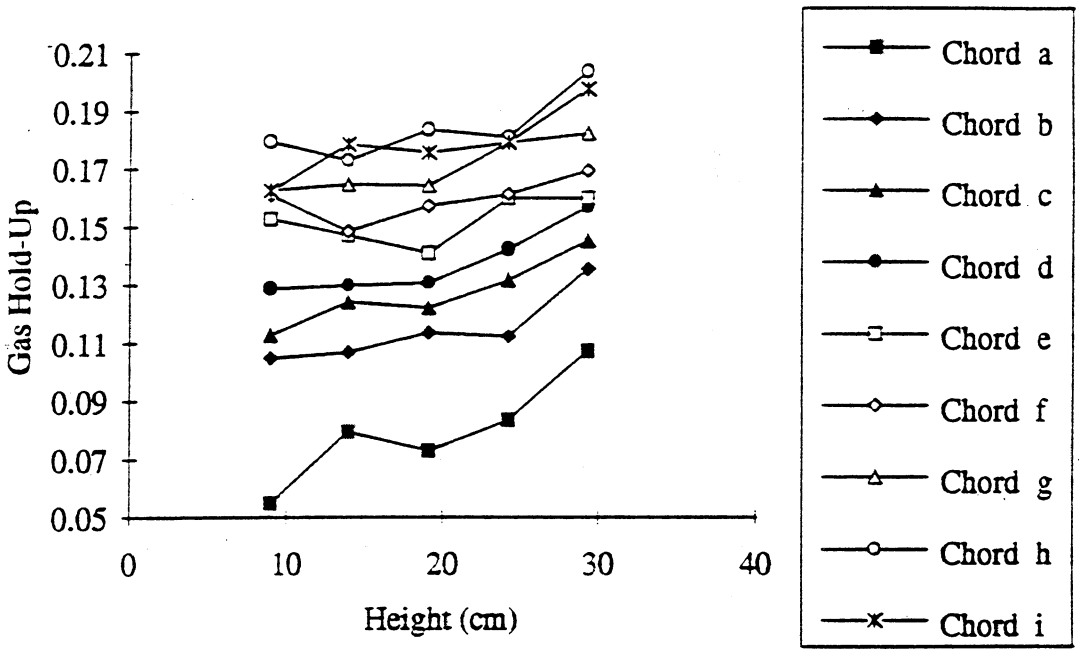

Gas holdup profiles in 1% consistency pulp, quiescent liquid apparatus.

Figure 6d. j_G = 5.26 cm/s

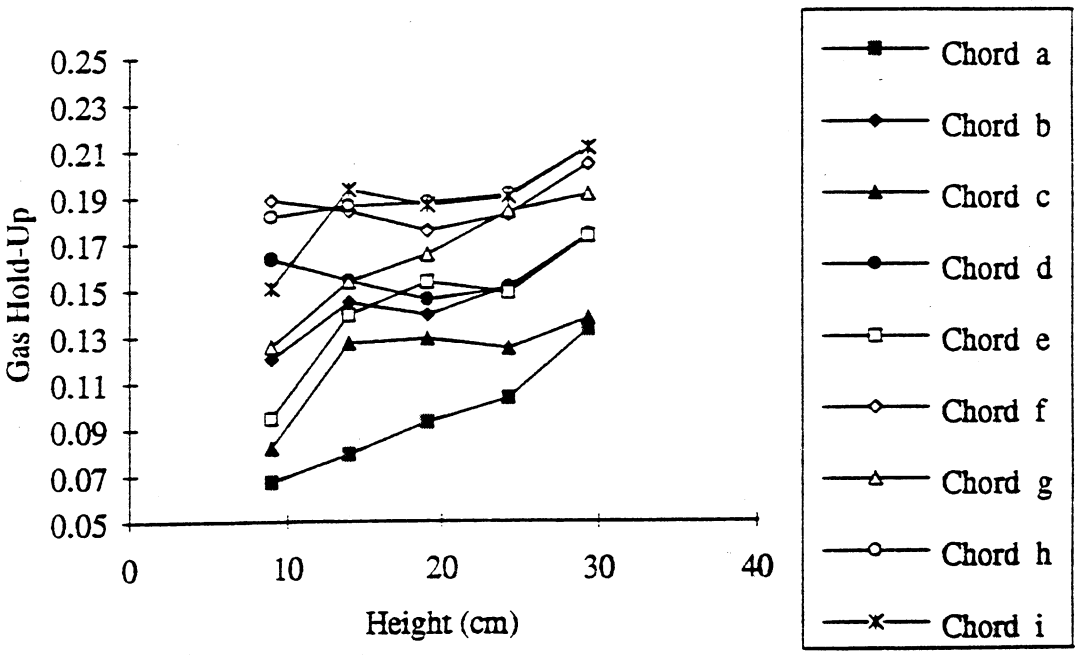

Gas holdup profiles in 1% consistency pulp, quiescent liquid apparatus.

Figure 6e. j_G = 6.58 cm/s

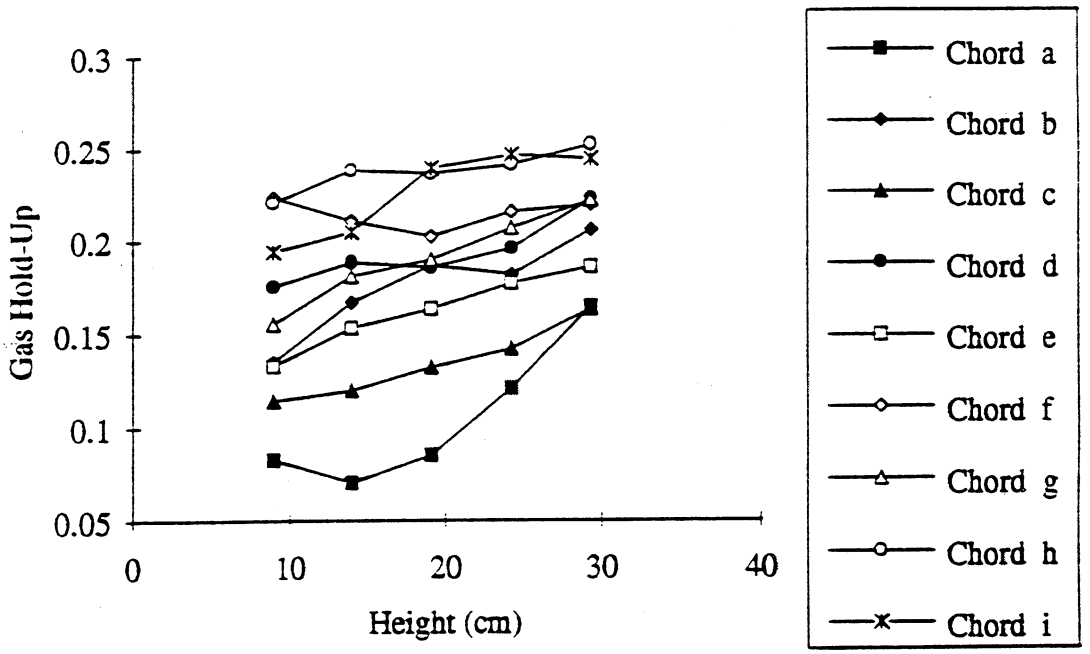

Gas holdup profiles in 1% consistency pulp, quiescent liquid apparatus.

Figure 6f. j_G = 9.21 cm/s

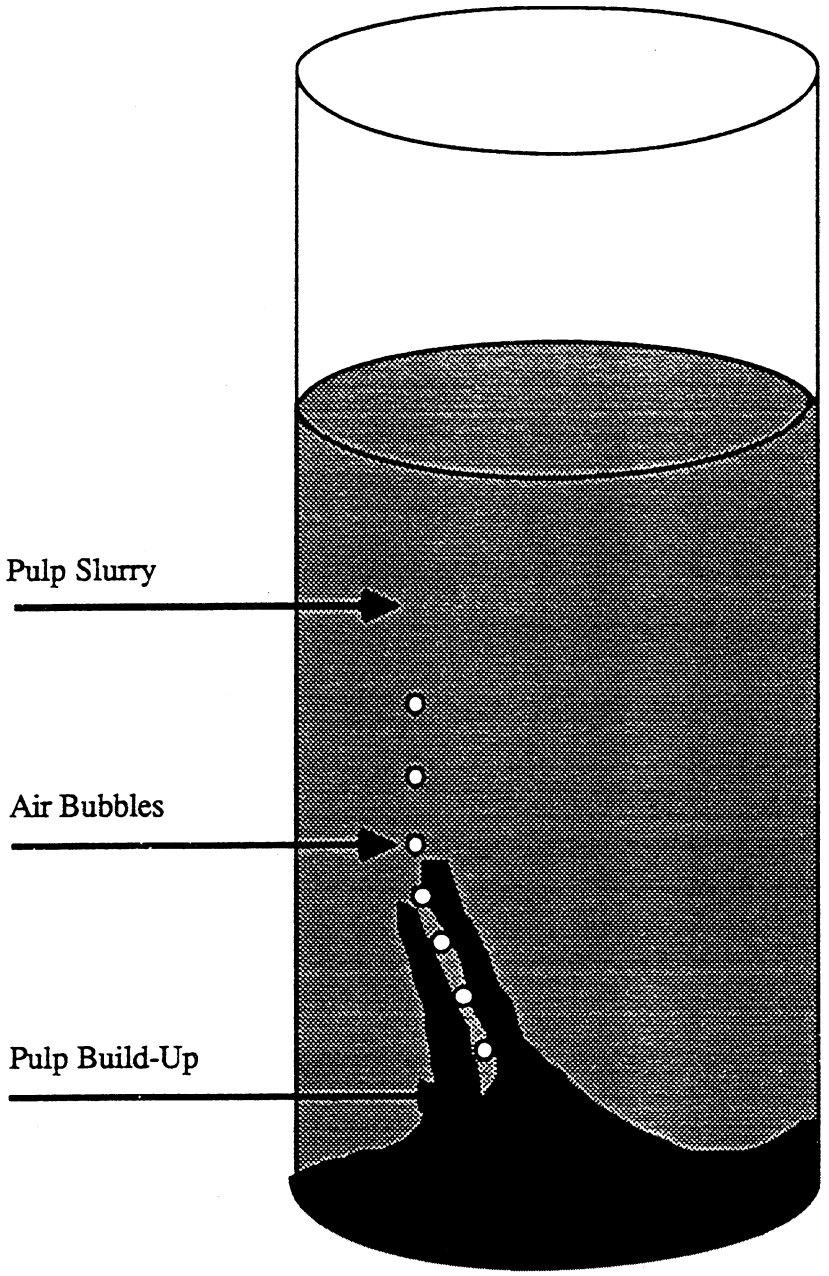

Figure 7. Typical pulp build-up formation in 1% consistency tests, quiescent liquid apparatus (not drawn to scale).

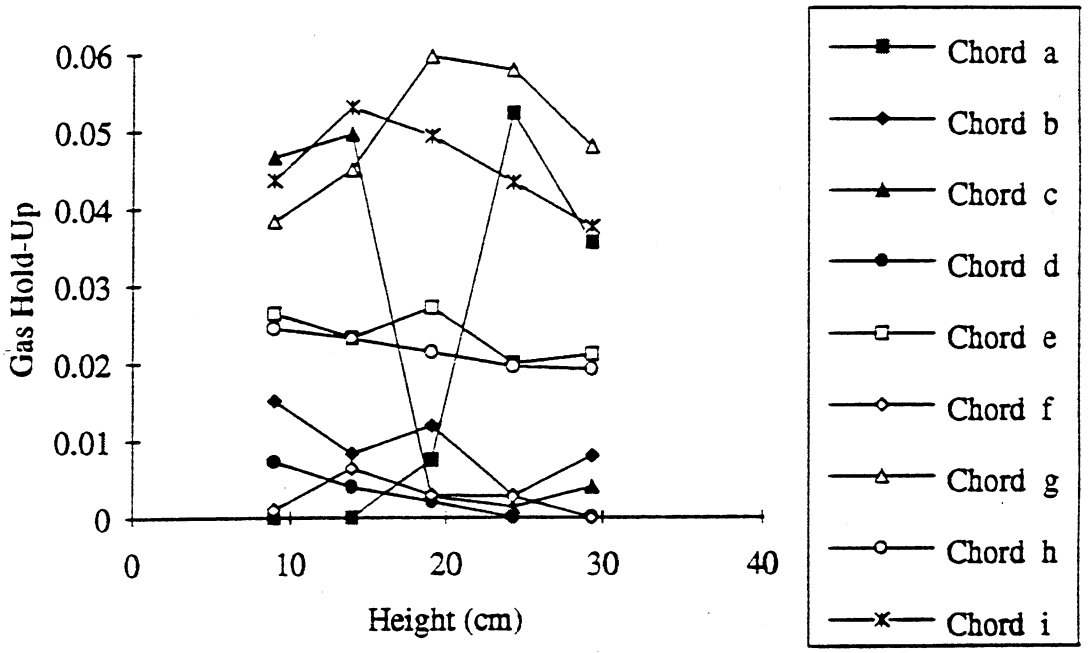

Gas holdup profiles in 2% consistency pulp, quiescent liquid apparatus.

Figure 8a. j_G = 0.79 cm/s

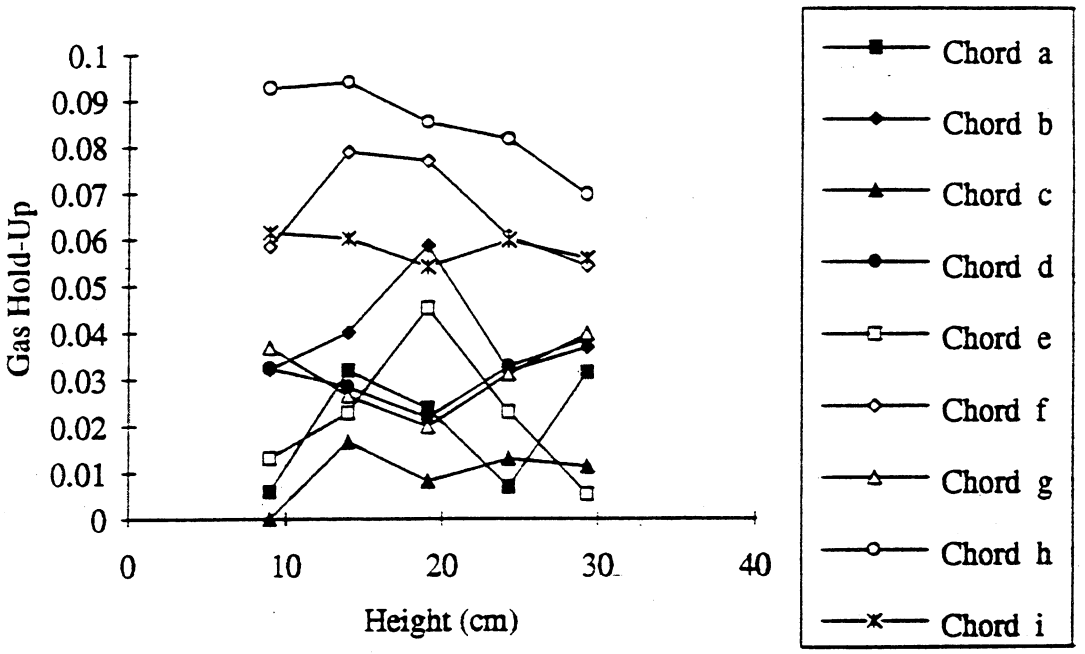

Gas holdup profiles in 2% consistency pulp, quiescent liquid apparatus.

Figure 8b. j_G = 1.32 cm/s

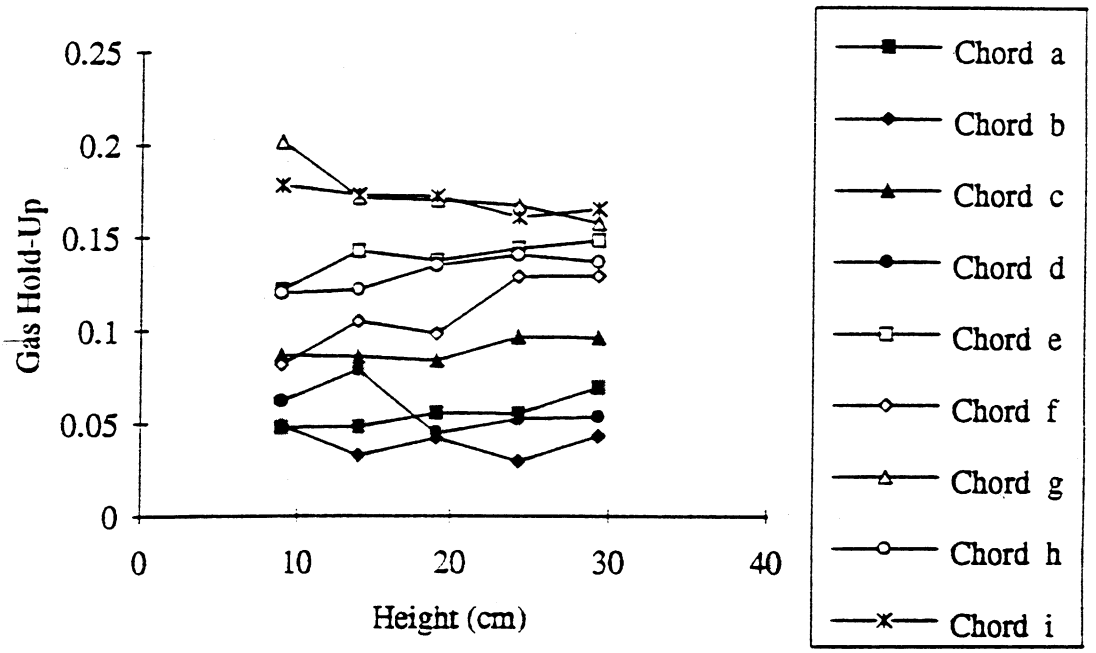

Gas holdup profiles in 2% consistency pulp, quiescent liquid apparatus.

Figure 8c. j_G = 3.95 cm/s

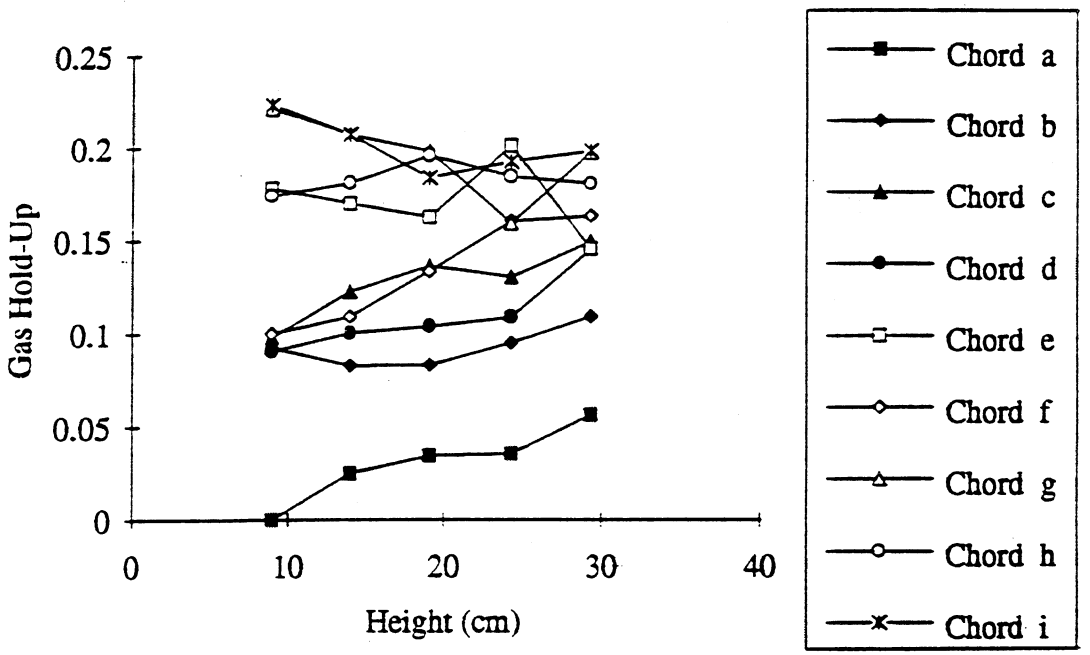

Gas holdup profiles in 2% consistency pulp, quiescent liquid apparatus.

Figure 8d. j_G = 5.26 cm/s

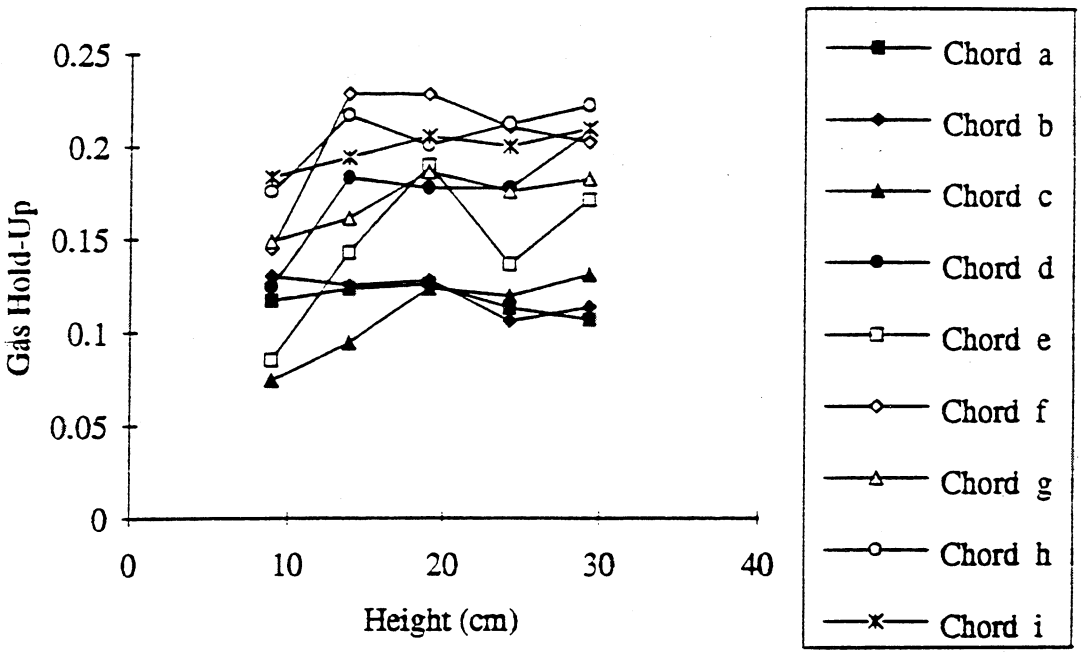

Gas holdup profiles in 2% consistency pulp, quiescent liquid apparatus.

Figure 8e. j_G = 6.58 cm/s

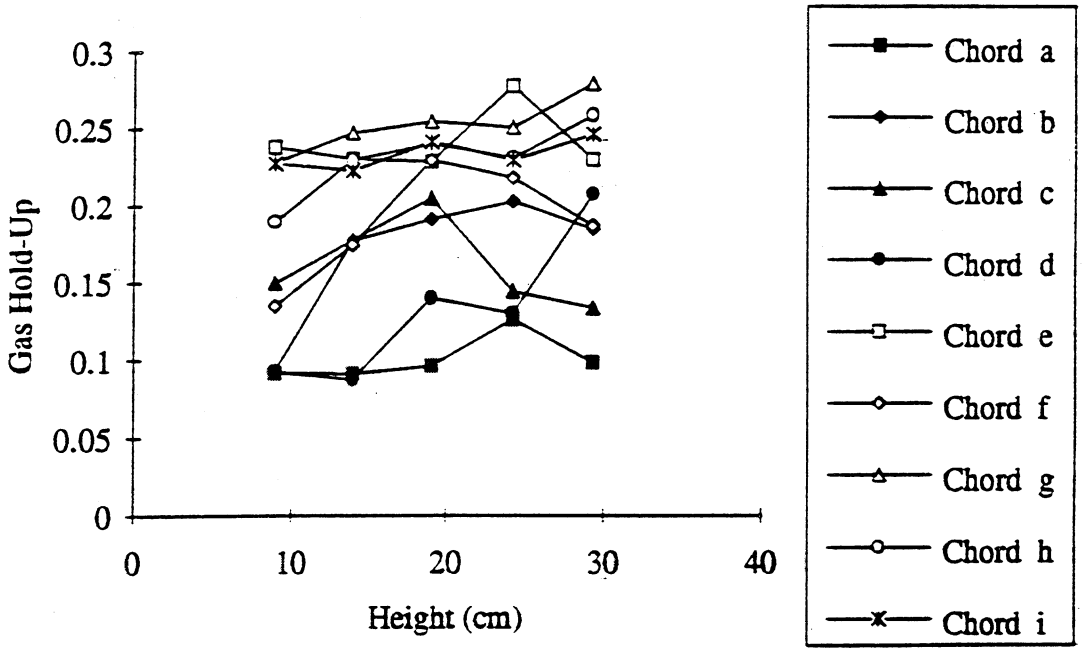

Gas holdup profiles in 2% consistency pulp, quiescent liquid apparatus.

Figure 8f. j_G = 9.21 cm/s

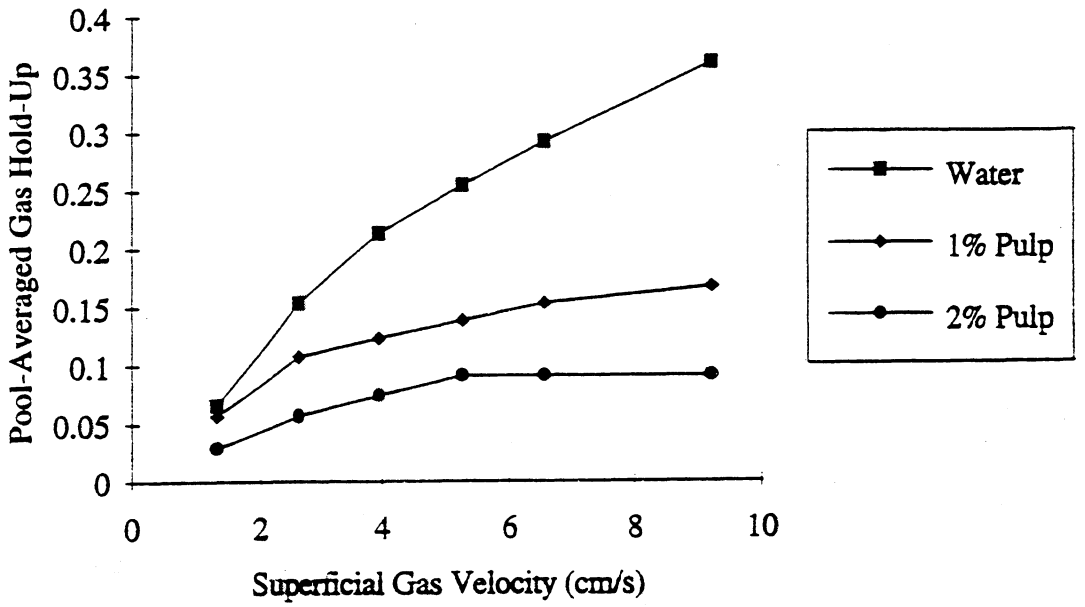

Figure 9. Pool-averaged gas holdup based on swell level height (quiescent liquid apparatus).

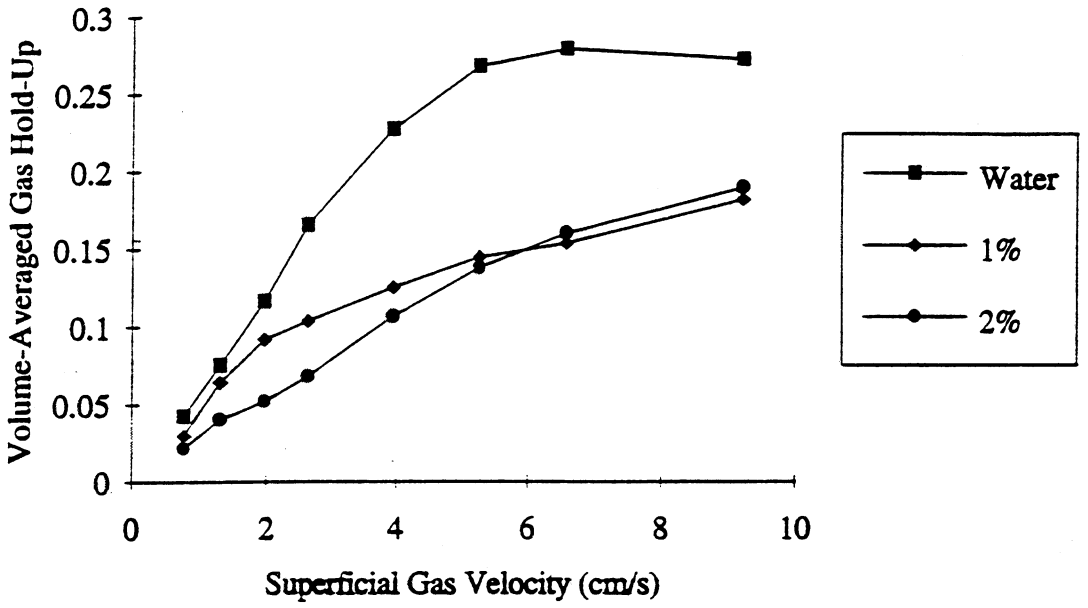

Figure 10. Pool-averaged gas holdup based on gamma densitometry measurements (quiescent liquid apparatus).

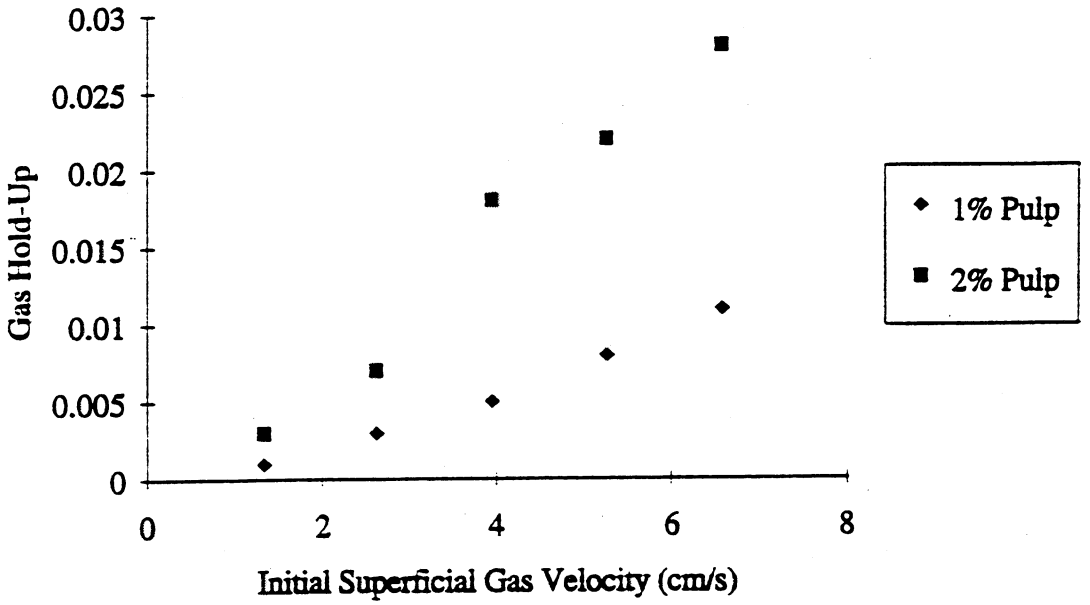

Figure 11. Residual gas holdup.

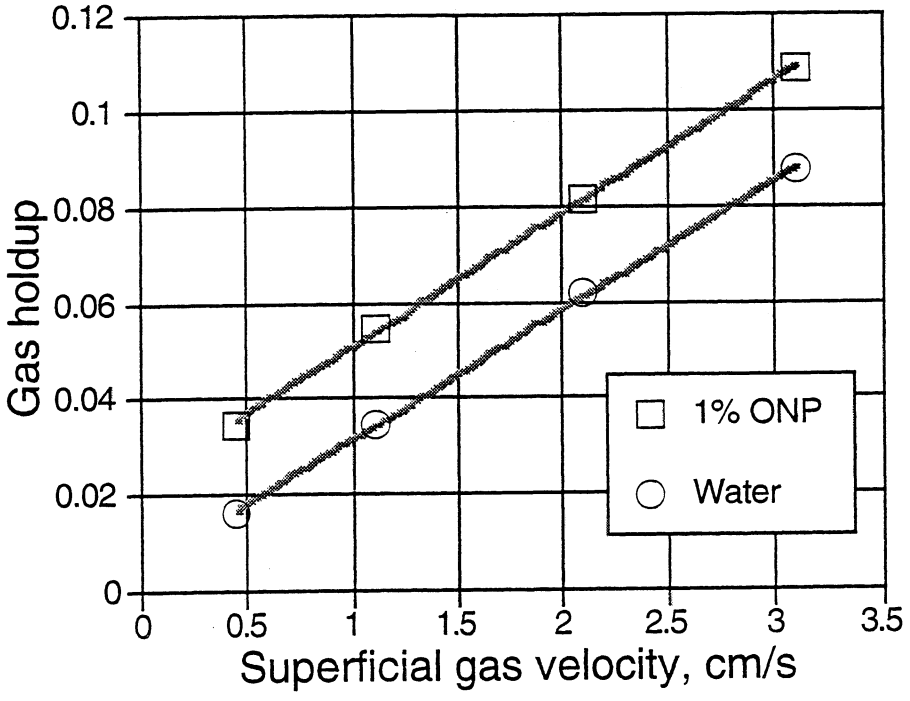

Figure 12. Column averaged gas holdup in 1% ONP and in water as a function of gas flux for a constant superficial velocity of 2.5 cm/s (5 gpm).

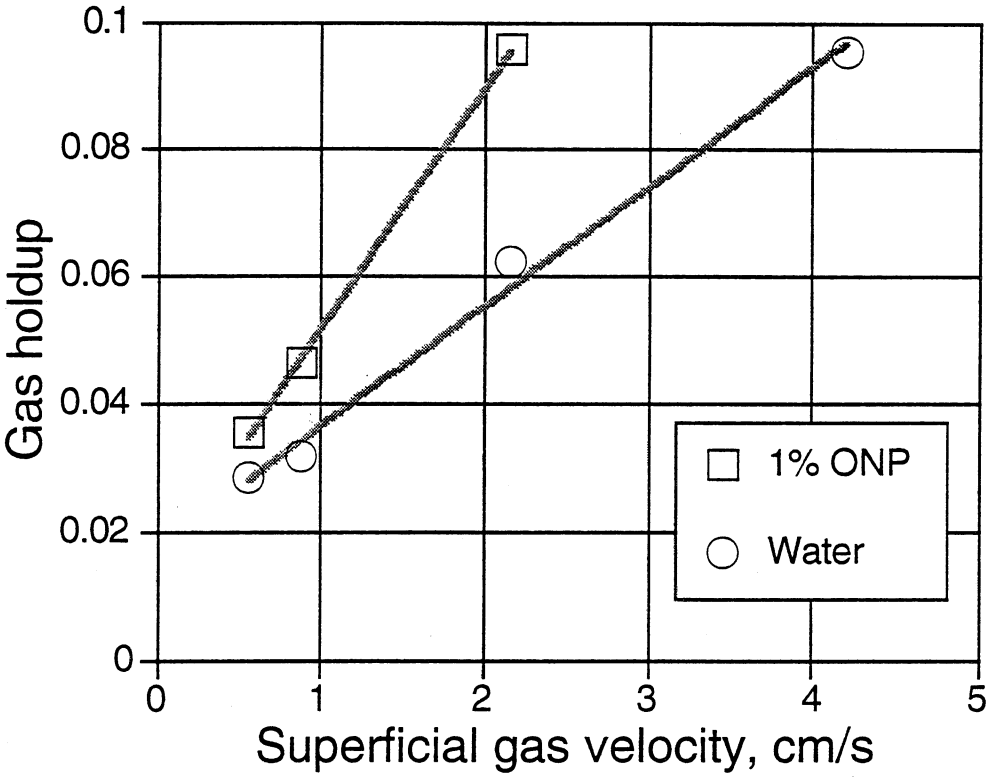

Figure 13. Column averaged gas holdup in 1% ONP and in water as a function of gas flux for a constant superficial velocity of 5.1 cm/s (10 gpm).

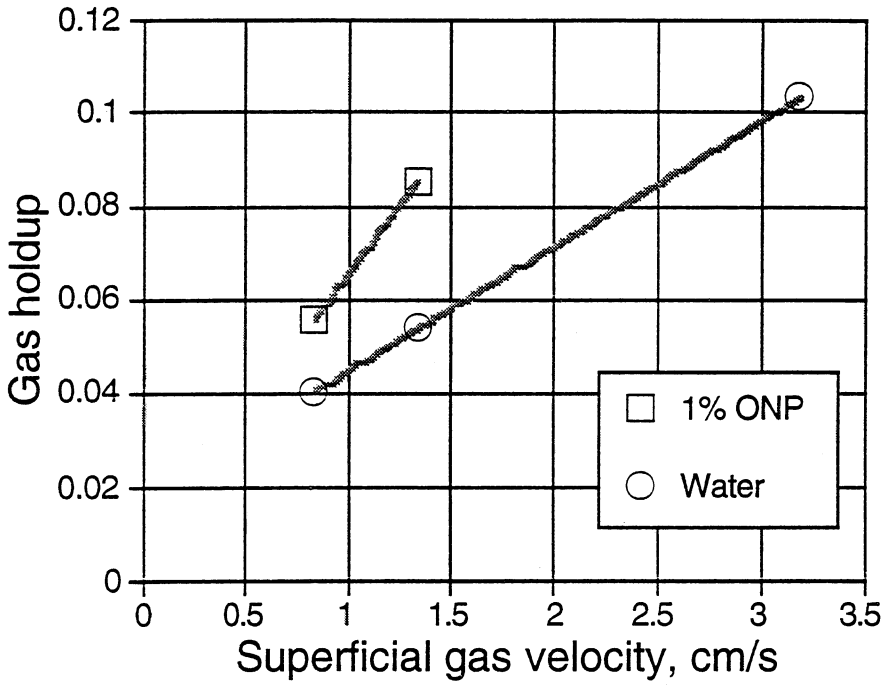

Figure 14. Column averaged gas holdup in 1% ONP and in water as a function of gas flux for a constant superficial velocity of 7.6 cm/s (15 gpm).

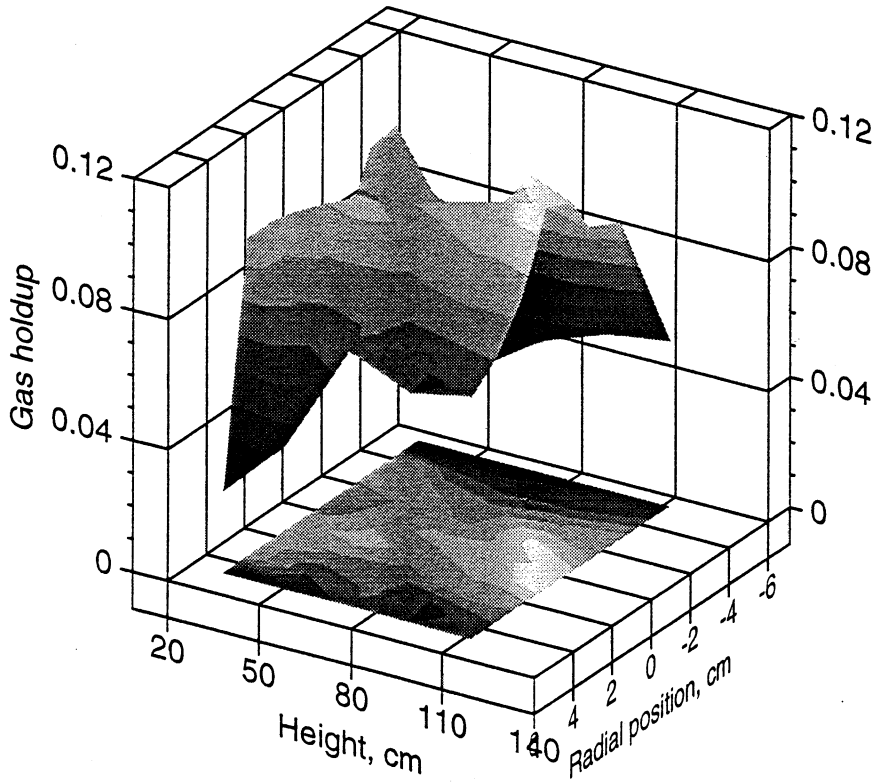

Figure 15. Chord-averaged gas holdup in the cocurrent flow system for water with superficial velocities of 2.5 cm/s for water and 3.1 cm/s for air.

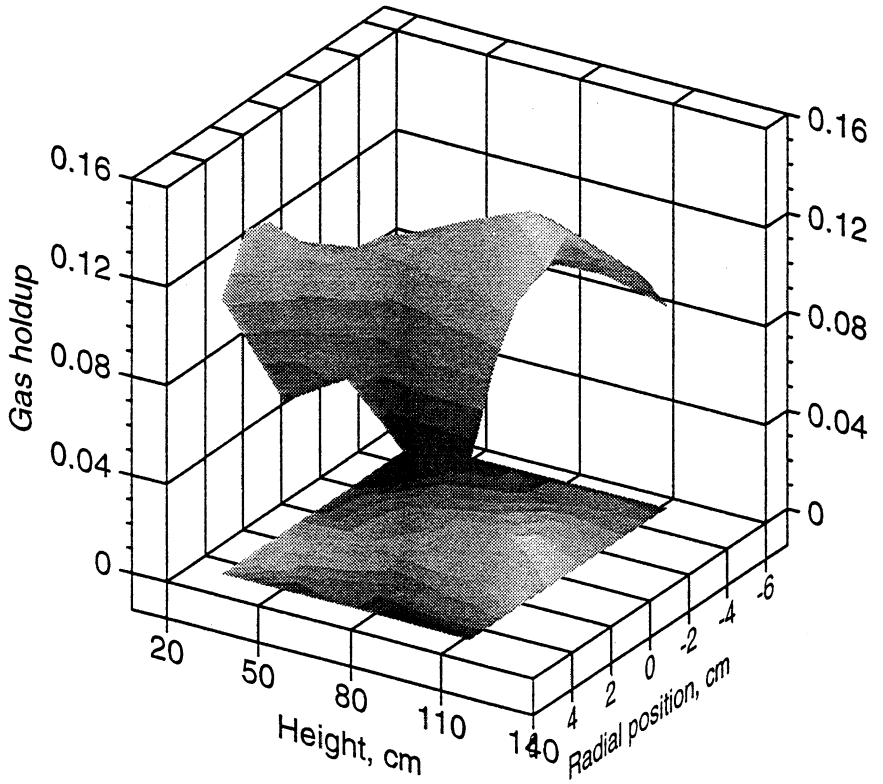

Figure 16. Chord-averaged gas holdup in the cocurrent flow system for 1% ONP with superficial velocities of 2.5 cm/s for pulp and 3.1 cm/s for air.

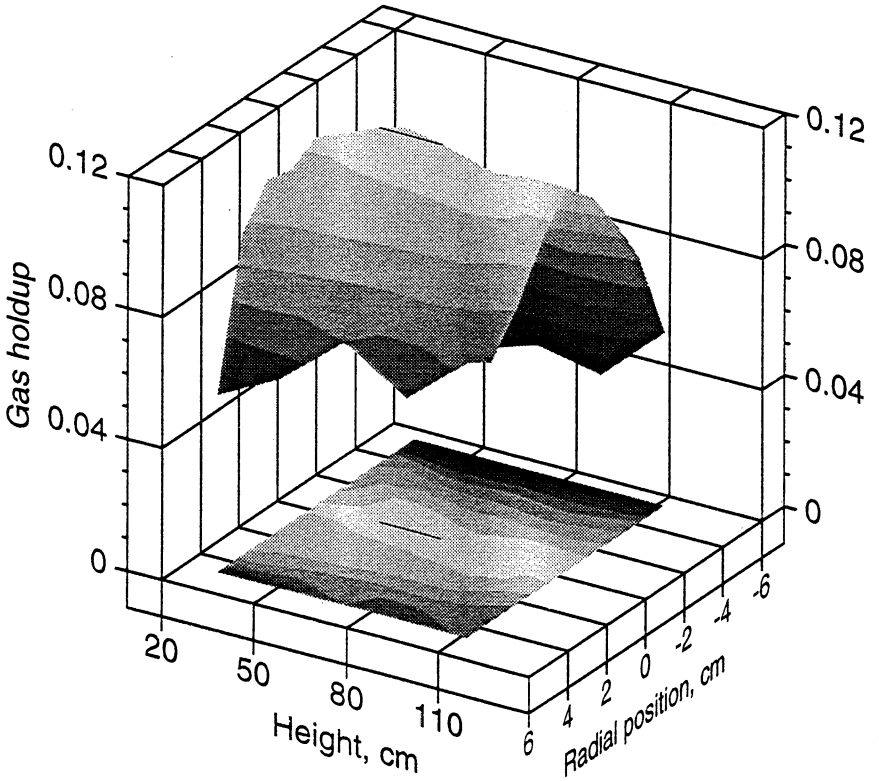

Figure 17. Chord-averaged gas holdup in the cocurrent flow system for water with superficial velocities of 5.1 cm/s for water and 2.16 cm/s for air.

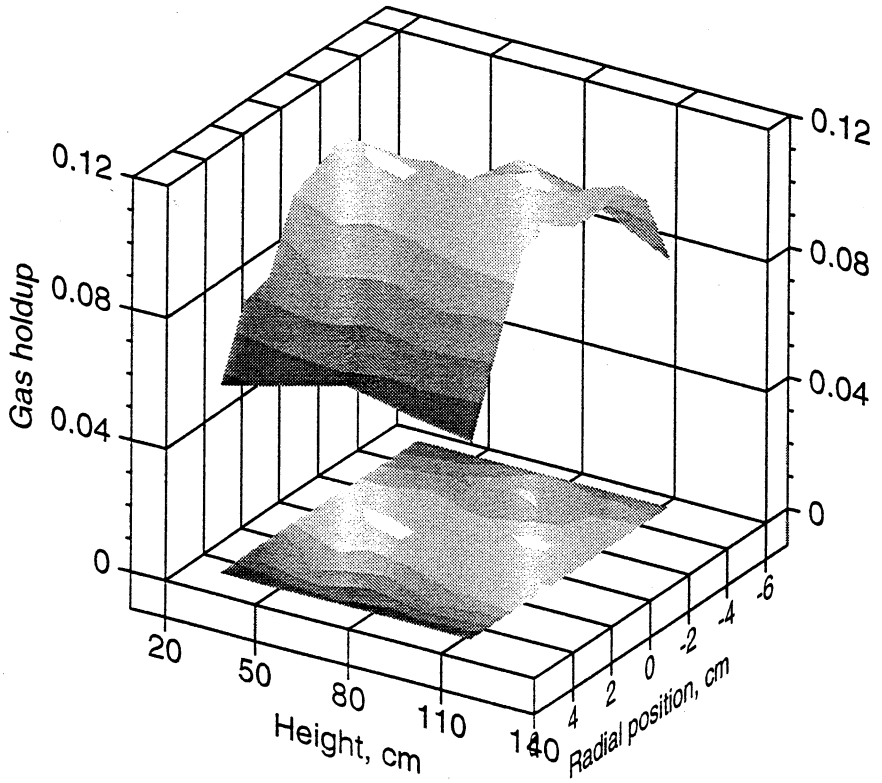

Figure 18. Chord-averaged gas holdup in the cocurrent flow system for 1% ONP with superficial velocities of 5.1 cm/s for pulp and 2.16 cm/s for air.

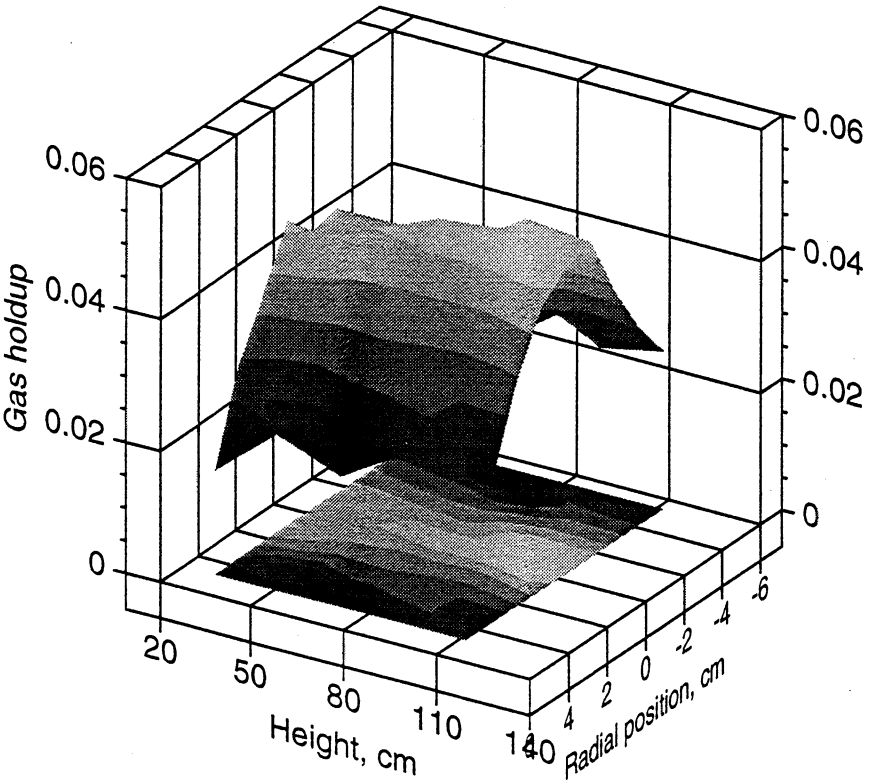

Figure 19. Chord-averaged gas holdup in the cocurrent flow system for 1% ONP with superficial velocities of 5.1 cm/s for pulp and 0.56 cm/s for air.